The Astronomical Journal, 134:2435–2450, 2007 December

FOUR QUASARS ABOVE REDSHIFT 6 DISCOVERED BY THE CANADA-FRANCE HIGH-z QUASAR SURVEY

Chris J. Willott,[1] Philippe Delorme,[2] Alain Omont,[3] Jacqueline Bergeron,[3] Xavier Delfosse,[2] Thierry Forveille,[2]
Loic Albert,[4] Céline Reylé,[5] Gary J. Hill,[6] Michael Gully-Santiago,[6] Phillip Vinten,[1]
David Crampton,[7] John B. Hutchings,[7] David Schade,[7] Luc Simard,[7]
Marcin Sawicki,[8] Alexandre Beelen,[9] and Pierre Cox[10]
Received 2007 May 29; accepted 2007 August 28

ABSTRACT

The Canada-France High-z Quasar Survey (CFHQS) is an optical survey designed to locate quasars during the epoch of reionization. In this paper we present the discovery of the first four CFHQS quasars at redshifts greater than 6, including the most distant known quasar, CFHQS J2329−0301 at $z = 6.43$. We describe the observational method used to identify the quasars and present optical, infrared, and millimeter photometry and optical and near-infrared spectroscopy. We investigate the dust properties of these quasars, finding an unusual dust extinction curve for one quasar and a high far-infrared luminosity due to dust emission for another. The mean millimeter continuum flux for CFHQS quasars is substantially lower than that for SDSS quasars at the same redshift, likely due to a correlation with quasar UV luminosity. For two quasars with sufficiently high signal-to-noise ratio optical spectra, we use the spectra to investigate the ionization state of hydrogen at $z > 5$. For CFHQS J1509−1749 at $z = 6.12$ we find significant evolution (beyond a simple extrapolation of lower redshift data) in the Gunn-Peterson optical depth at $z > 5.4$. The line of sight to this quasar has one of the highest known optical depths at $z \approx 5.8$. An analysis of the sizes of the highly ionized near-zones in the spectra of two quasars at $z = 6.12$ and 6.43 suggest that the intergalactic medium surrounding these quasars was substantially ionized before these quasars turned on. Together, these observations point toward an extended reionization process, but we caution that cosmic variance is still a major limitation in $z > 6$ quasar observations.

Key words: cosmology: observations — intergalactic medium — quasars: absorption lines — quasars: emission lines — quasars: general

Online material: color figures

1. INTRODUCTION

The earliest observed epoch of the universe is 380,000 yr after the big bang, when protons and electrons combined into neutral hydrogen. The radiation from this epoch, observed as the cosmic microwave background, shows that the universe was homogeneous with fractional density fluctuations of only $\sim 10^{-4}$. For the following few hundred million years there were no stars or galaxies. This period is often referred to as the "dark ages" because of the absence of sources of light (Rees 1999).

Eventually these small density fluctuations in the dark matter distribution grew into dark matter halos, where gas could cool and form galaxies. As stars and black holes formed within galaxies they emitted copious amounts of ultraviolet (UV) radiation. Many of these photons escaped their host galaxies and ionized hydrogen in the intergalactic medium (IGM). When sufficient sources of ionizing photons had formed, they provided an ionizing background radiation field high enough to ionize all the diffuse neutral hydrogen in the IGM. The details of reionization are sensitive to the luminosity function of ionizing sources, the fraction of ionizing photons that escape from them, the ionizing source spectra, and the clumpiness of the IGM (Miralda-Escudé et al. 2000).

Quasars are useful probes of reionization because they can be detected at very high redshift and have strong intrinsic UV radiation that is absorbed at the resonant Lyman lines by neutral hydrogen. The presence of significant flux in the Lyα forest of quasars at $z < 6$ indicates that the IGM is almost completely reionized by this epoch (Fan et al. 2000, 2001; Songaila 2004). The discovery of Gunn-Peterson troughs in the spectra of quasars at $6 < z < 6.42$ has been interpreted as evidence that we are approaching the epoch of reionization (Becker et al. 2001; White et al. 2003; Fan et al. 2006a). Fan et al. (2006b) analyzed a sample of 19 SDSS quasars at $z > 5.7$ and found that the mean Gunn-Peterson optical depth and its variance increase sharply away from the low-redshift extrapolation at $z > 5.7$, consistent with the overlap phase of reionization occurring at $z \approx 6.1$ (Gnedin & Fan 2006). However, it has also been argued that these data are compatible with much earlier reionization (Songaila 2004; Becker et al. 2007).

The sizes of highly ionized near-zones around quasars are sensitive to the neutral fraction of hydrogen before the quasar turned on (Cen & Haiman 2000). However, the interpretation of these results is complex, and various authors have come to a wide range of conclusions on the basis of the same SDSS quasar spectra (Wyithe & Loeb 2004; Wyithe et al. 2005; Yu & Lu 2005; Fan et al. 2006b; Bolton & Haehnelt 2007a, 2007b; Mesinger &

[1] Physics Department, University of Ottawa, 150 Louis Pasteur, MacDonald Hall, Ottawa, ON K1N 6N5, Canada; cwillott@uottawa.ca.
[2] Laboratoire d'Astrophysique, Observatoire de Grenoble, Université J. Fourier, BP 53, F-38041 Grenoble, Cedex 9, France.
[3] Institut d'Astrophysique de Paris-CNRS, 98bis Boulevard Arago, F-75014 Paris, France.
[4] Canada-France-Hawaii Telescope Corporation, 65-1238 Mamalahoa Highway, Kamuela, HI 96743, USA.
[5] Institut Utinam, Observatoire de Besançon, BP 1615, F-25010 Besançon Cedex, France.
[6] McDonald Observatory, University of Texas at Austin, 1 University Station, Austin, TX 78712, USA.
[7] Herzberg Institute of Astrophysics, National Research Council, 5071 West Saanich Road, Victoria, BC V9E 2E7, Canada.
[8] Department of Astronomy and Physics, St. Mary's University, 923 Robie Street, Halifax, NS B3H 3C3, Canada.
[9] Institut d'Astrophysique Spatiale, Université Paris-Sud, F-91405 Orsay Cedex, France.
[10] Institute de Radioastronomie Millimetrique, F-38406 St. Martin d'Heres, France.

Haiman 2007; Alvarez & Abel 2007). Despite these uncertainties, this could be a powerful probe at high neutral fractions where traditional Gunn-Peterson measurements are insensitive. Becker et al. (2006) studied O I absorption up to $z = 6.42$ and did not find an O I forest, suggesting that these lines of sight are either largely unenriched or significantly ionized.

Simulations predict that reionization is an inhomogeneous process due to the existence of discrete, clustered ionizing sources and an inhomogeneous IGM (e.g., Barkana & Loeb 2001). Cosmic variance in transmission due to large-scale density inhomogeneities is extremely large on proper scales up to 20 Mpc at $z = 5.5$ and rapidly increases at earlier times before full reionization (Wyithe & Loeb 2006). The SDSS currently contains only a handful of quasars at a high enough redshift ($z > 6.1$) to probe a large path length of the $z > 6$ IGM. From Fan et al. (2006a) and references therein, the path length at $z > 6$ currently probed by the SDSS quasars is only ~40 proper Mpc (excluding the broad absorption line quasar SDSS J1048+4607, whose broad absorption lines may be confused with IGM absorption). Observations of SDSS quasars at $z > 6.2$ show evidence for significant cosmic variance with a substantial range of foreground IGM absorption (Oh & Furlanetto 2005). More quasars are required to overcome cosmic variance at $z > 6$.

Observations of high-redshift quasars are important for studying not only reionization, but also the formation of supermassive black holes and their host galaxies. The high luminosities and broad line widths of the most distant quasars require black holes with masses greater than $10^9\ M_\odot$ (Fan et al. 2001; Willott et al. 2003). Forming such massive black holes within the first billion years of the universe provides a challenge to models of galaxy formation, black hole formation, and black hole growth (Bromley et al. 2004; Yoo & Miralda-Escudé 2004; Shapiro 2005; Volonteri & Rees 2005; King & Pringle 2006).

It is well established that there is a tight relation between the mass of the black hole and the spheroid in local galaxies (Magorrian et al. 1998). However, the evolution of this relation with redshift is not well known, and attempts are now being made to determine the relation up to $z = 3$ because it is a crucial component of galaxy evolution models (Shields et al. 2003; Adelberger & Steidel 2005; Alexander et al. 2005; Peng et al. 2006; McLure et al. 2006). It is also important to push this relation out to $z \sim 6$, where the earliest known black holes exist. Studies of millimeter radiation show that at least 40% of $z \sim 6$ quasars have high far-infrared luminosities indicative of high star formation rates of $\sim 1000\ M_\odot\ \mathrm{yr}^{-1}$ (Wang et al. 2007). SDSS J1148+5251 has resolved CO emission, making it the only $z > 6$ quasar with a dynamical mass measurement (Walter et al. 2004). Curiously, the mass inferred is an order of magnitude less than expected if there is no evolution in the black hole–spheroid relation.

To date, only 10 quasars have been discovered at redshifts greater than or equal to 6 (Fan et al. 2006a and references therein; McGreer et al. 2006). To discover more very distant quasars which can be used as probes of reionization and the early growth of massive black holes and galaxies, we are carrying out the Canada-France High-z Quasar Survey (CFHQS). This project uses the 1 deg^2 imager MegaCam at the Canada-France-Hawaii Telescope (CFHT). The survey plans to cover ~900 deg^2 in the four optical filters g', r', i', and z' to a limiting depth of $z' \approx 22.5$. This is more than 2 mag fainter than the SDSS survey, leading to the discovery of correspondingly lower luminosity quasars. Lower luminosity quasars are expected to have lower black hole masses, which could be due to the black holes being younger than those in SDSS quasars. The survey is carried out in areas of the sky which already have MegaCam imaging in some filters as part of the CFHT Legacy Survey[11] or the Red Sequence Cluster Survey 2.[12] As discussed below, the survey is also extremely effective at finding ultracool brown dwarfs. In this paper we present the first high-redshift quasars to be discovered in the CFHQS.

In the following section we describe how the quasars were discovered from imaging and spectroscopic observations. Section 3 presents the properties of the four quasars. Section 4 deals with observations at other wavelengths, including millimeter observations. In § 5 we discuss constraints on the ionization state of hydrogen at high redshift from these quasars. Section 6 presents our conclusions.

All optical and near-IR magnitudes in this paper are in the AB system. Cosmological parameters of $H_0 = 70$ km s^{-1} Mpc^{-1}, $\Omega_M = 0.27$, and $\Omega_\Lambda = 0.73$ (Spergel et al. 2007) are assumed throughout. The convention for spectral indices, α_ν, is that $f_\nu \propto \nu^{-\alpha_\nu}$.

2. OBSERVATIONS

2.1. *Imaging*

The four quasars whose discovery we report here were found in the first 2 years of optical imaging of the CFHQS. The total area covered at this time is ≈400 deg^2 to typical limits of $z' \approx 22.5$ and $i' \approx 24.5$. However, because follow-up observations are not complete, we expect this region to contain more quasars than discovered so far, and no conclusions on the space density of low-luminosity quasars and the shape of the luminosity function at $z = 6$ are available at this time.

We only briefly describe the processing and photometry of the imaging observations in this paper. A much fuller description is given in P. Delorme et al. (2008, in preparation). Preprocessing of the MegaCam images is carried out at CFHT using the ELIXIR pipeline. This removes the instrumental effects from the images. We then run our own algorithms to improve the astrometry and check the photometry. Finally, we stack the images (for those cases where there is more than one exposure at a given position) and register the images in the four different filters. Photometry is carried out using our own adaption of SExtractor (Bertin & Arnouts 1996), which uses dual-image multiple point-spread function fitting (P. Delorme & E. Bertin 2008, in preparation) to optimize the signal-to-noise ratio (S/N) of point sources.

Candidate quasars are initially identified on the optical images as objects which have very high $i' - z'$ colors. In Willott et al. (2005a) we described in detail our method for identifying high-z quasars and brown dwarfs using MegaCam optical plus near-IR imaging. As shown in that paper, photometric noise causes many M stars (with intrinsic colors of $0.5 < i' - z' < 1$) to be scattered into the region of the diagram at $i' - z' > 1.5$ where we would expect to find only L or T dwarfs and quasars. The huge number of these M stars would require a lot of telescope time for complete follow-up. Therefore, we now limit our survey to objects observed to be redder than $i' - z' > 1.7$, with stronger priority for follow-up given to redder objects. In Willott et al. (2005a) we showed that changing the criterion from $i' - z' > 1.5$ to $i' - z' > 1.7$ only loses us quasars at $z < 5.9$, but reduces the number of M dwarf contaminants by >80%. Similarly, imposing a cut at $i' - z' > 1.8$ or even $i' - z' > 2$ would have very little effect on the number of $z > 6$ quasars discovered. All of the quasars presented in this paper were observed to have $i' - z' > 2$.

To separate quasars from brown dwarfs we employ near-infrared J-band imaging (e.g., Fan et al. 2001). Quasars at $z < 6.5$

[11] See http://www.cfht.hawaii.edu/Science/CFHTLS.
[12] See http://www.rcs2.org.

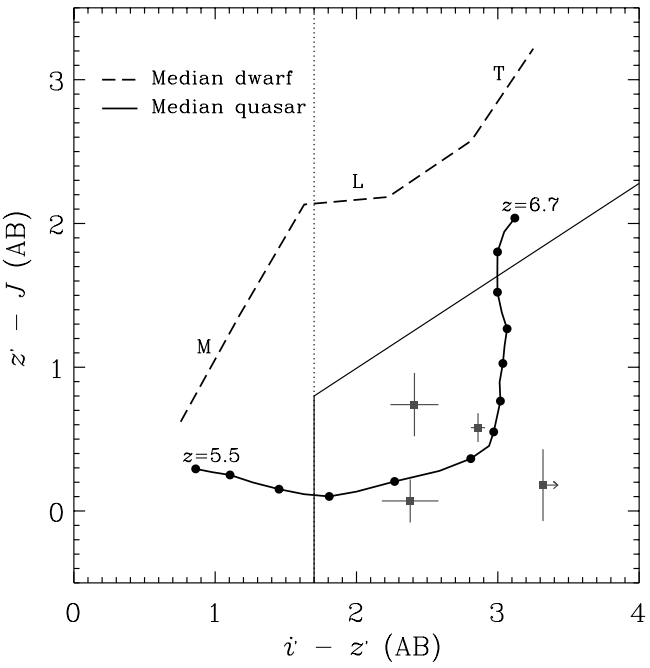

FIG. 1.—Color-color diagram showing the selection region for high-z quasars (to the lower right of the thin solid line). The thin dotted line shows the optical criterion of $i' - z' > 1.7$, which also allows many L and T dwarfs. The thick solid line is the median cloned quasar track for quasars at $5.5 < z < 6.7$, with a mark every $\delta z = 0.1$ (from Willott et al. 2005a). The thick dashed line is the median brown dwarf track for types M, L, and T. The four squares with error bars are the four new $z > 6$ quasars. Colors of the brown dwarfs discovered by this survey will be presented in P. Delorme et al. (2008, in preparation). [*See the electronic edition of the Journal for a color version of this figure.*]

appear relatively blue in $z' - J$, whereas L and T dwarfs are very red. Near-IR imaging was carried out at several telescopes, and the observations, processing, and photometry are described in P. Delorme et al. (2008, in preparation).

Figure 1 shows the $i' - z'$ versus $z' - J$ color-color diagram for the newly discovered quasars. Also shown are lines corresponding to the expected median colors of quasars at redshifts $5.5 < z < 6.7$ and the median track for brown dwarfs discovered by 2MASS and SDSS. The expected quasar color track is based on "cloning" of 180 SDSS quasars at $z = 3$ (see Willott et al. 2005a for full details). Three of the quasars lie very close to the median quasar track. The exception is CFHQS J2329−0301, which is much redder in $i' - z'$ and bluer in $z' - J$ than expected given its redshift. The reason for this will be discussed in § 3. Positions and photometry for the four quasars are given in Table 1.

In Figure 2 are shown $20'' \times 20''$ images centered on the quasars. All quasars are clearly detected at the z' band, but most have only faint detections at i' and J. CFHQS J2329−0301 is the only quasar not detected at i'. CFHQS J1509−1749 is fortuitously located only $12''$ from a very bright ($R = 12.6$) star and is ideally suited to natural guide-star adaptive-optics observations. Finding charts in the z' band over a wider field are presented in the Appendix.

2.2. *Spectroscopy*

Optical spectroscopy of candidate quasars was carried out using the Gemini Multi-Object Spectrograph (GMOS; Hook et al. 2004) at the Gemini South Telescope and the Marcario Low Resolution Spectrograph (LRS; Hill et al. 1998) at the Hobby-Eberly Telescope. The details of these observations are given in Table 2.

The GMOS spectroscopy was carried out using the nod-and-shuffle mode to minimize sky-subtraction residuals at the red end of the spectra. Most of the reductions of the Gemini spectra were performed using tasks in the IRAF Gemini package, which were specifically designed for GMOS. The first step is removal of the bias level using a bias frame constructed from many (>10) bias observations (with the same binning) carried out during the same month. Then the sky is removed from the spectra by subtracting a spectrum of the sky obtained through exactly the same light path. GMOS consists of three separate chips, so the next step is to mosaic together the data on the three chips. Each object was observed in more than one exposure, so all exposures of each object were registered in the spectral direction using the location of night-sky emission lines (in unsubtracted images) and in the spatial direction using the location of the quasar spectrum or that of a bright star located along the slit. The registered exposures were combined using bad-pixel masks (including charge traps) and a sigma-clipping algorithm. The exposures of CFHQS J0033−0125 and CFHQS J2329−0301 each had only four spectra to combine, so a few cosmic rays survived and were manually edited out of the final two-dimensional spectra. Wavelength calibration was achieved using the night-sky spectrum from the unsubtracted images. The quasar spectra were then extracted from the two-dimensional spectra.

The LRS data reduction followed similar procedures. Cosmic rays were removed from the individual frames prior to co-addition with L.A.Cosmic (van Dokkum 2001). The wavelength scale was set, and the distortion removed from the frames with a combination of cadmium and neon lines. A fourth-order fit to the wavelength scale yields an accuracy of 1.0 Å or better from 6500 to 9100 Å. Incomplete fringing removal, beating with the night-sky lines, causes some residual positive features in the final spectrum. These are described further in § 3.

For the GMOS and LRS spectra, a relative flux calibration was applied using observations of a spectrophotometric standard star. Due to slit losses, absolute flux calibration was achieved by passing the spectra through the CFHT MegaCam z' filter + CCD response curves and normalizing to match the observed z' magnitudes.

The optical spectra of the four quasars are shown in Figure 3. In all four cases there is an unambiguous spectral break close to the Lyα emission line, indicating the object is a $z > 6$ quasar.

TABLE 1
POSITIONS AND PHOTOMETRY FOR THE CFHQS QUASARS

Quasar	R.A. (J2000.0)	Decl. (J2000.0)	i' (mag)	z' (mag)	J (mag)	$i' - z'$	$z' - J$
CFHQS J003311−012524.....	00 33 11.40	−01 25 24.9	24.82 ± 0.15	22.41 ± 0.08	21.58 ± 0.20	2.41 ± 0.17	0.74 ± 0.22
CFHQS J150941−174926.....	15 09 41.78	−17 49 26.8	23.11 ± 0.05	20.26 ± 0.02	19.68 ± 0.10	2.86 ± 0.05	0.58 ± 0.10
CFHQS J164121+375520.....	16 41 21.64	+37 55 20.5	23.69 ± 0.20	21.31 ± 0.04	21.24 ± 0.14	2.38 ± 0.20	0.07 ± 0.15
CFHQS J232908−030158.....	23 29 08.28	−03 01 58.8	>25.08[a]	21.76 ± 0.05	21.56 ± 0.25	>3.32	0.18 ± 0.25

NOTE.—Units of right ascension are hours, minutes, and seconds, and units of declination are degrees, arcminutes, and arcseconds.
[a] Where not detected at >2 σ significance, a 2 σ lower limit is given.

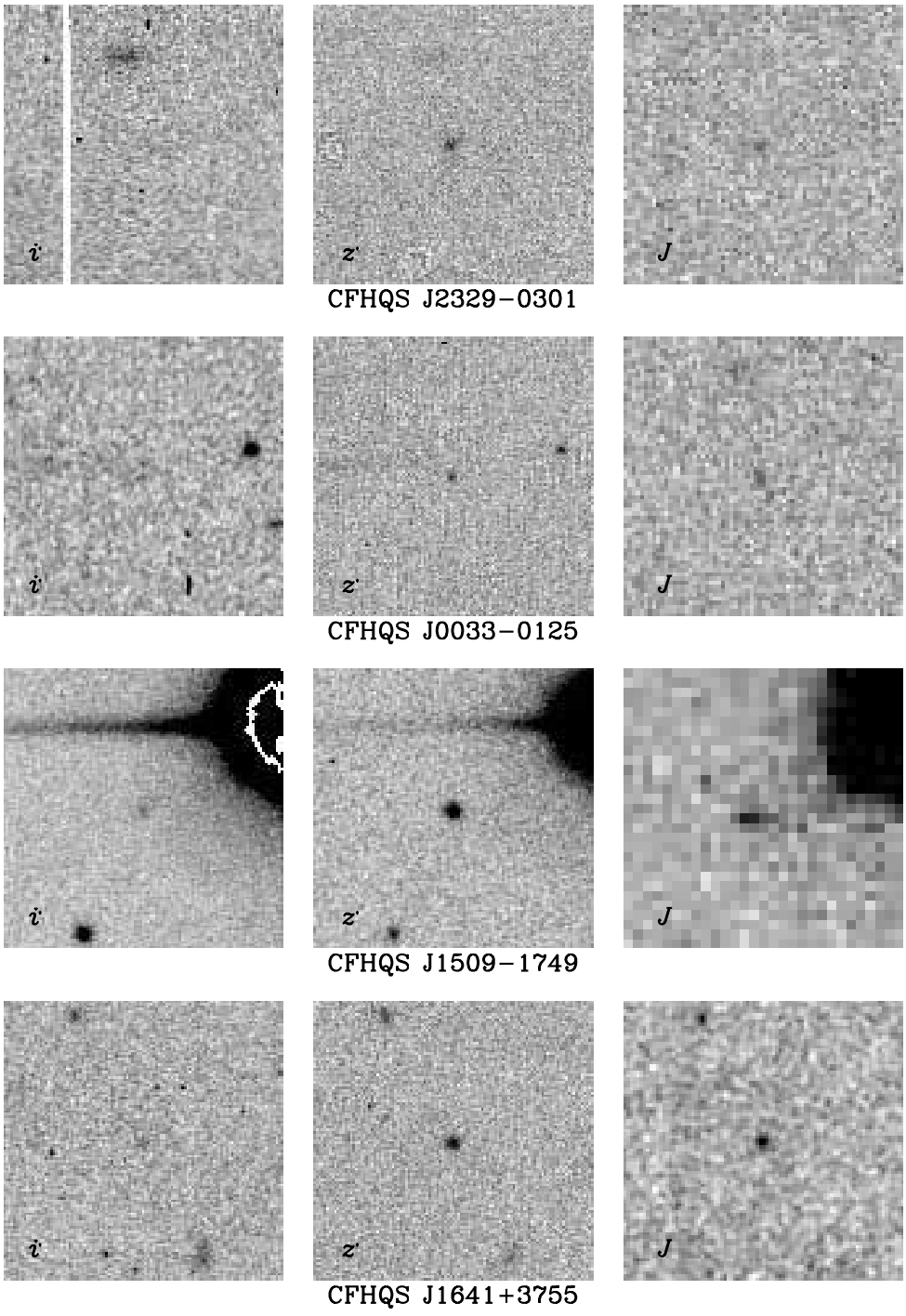

FIG. 2.—Images in the i', z', and J filters centered on the four CFHQS quasars. Each image covers $20'' \times 20''$. The images are oriented with north up and east to the left.

TABLE 2
OPTICAL SPECTROSCOPY OBSERVATIONS OF CFHQS QUASARS

Quasar	Redshift z	Telescope	Date	Resolving Power	Slit Width (arcsec)	Exp. Time (s)	Seeing (arcsec)	M_{1450}
CFHQS J0033−0125.....	6.13	Gemini	2006 Nov 26	1300	1.0	3600	0.6	−25.03
CFHQS J1509−1749.....	6.12	Gemini	2006 May 26	2100	0.5	7200	0.7	−26.98
CFHQS J1641+3755.....	6.04	HET	2006 Jul 26, Sep 19	400	2.0	5700	1.9	−25.48
CFHQS J2329−0301.....	6.43	Gemini	2006 Nov 26	1300	1.0	3600	0.7	−25.23

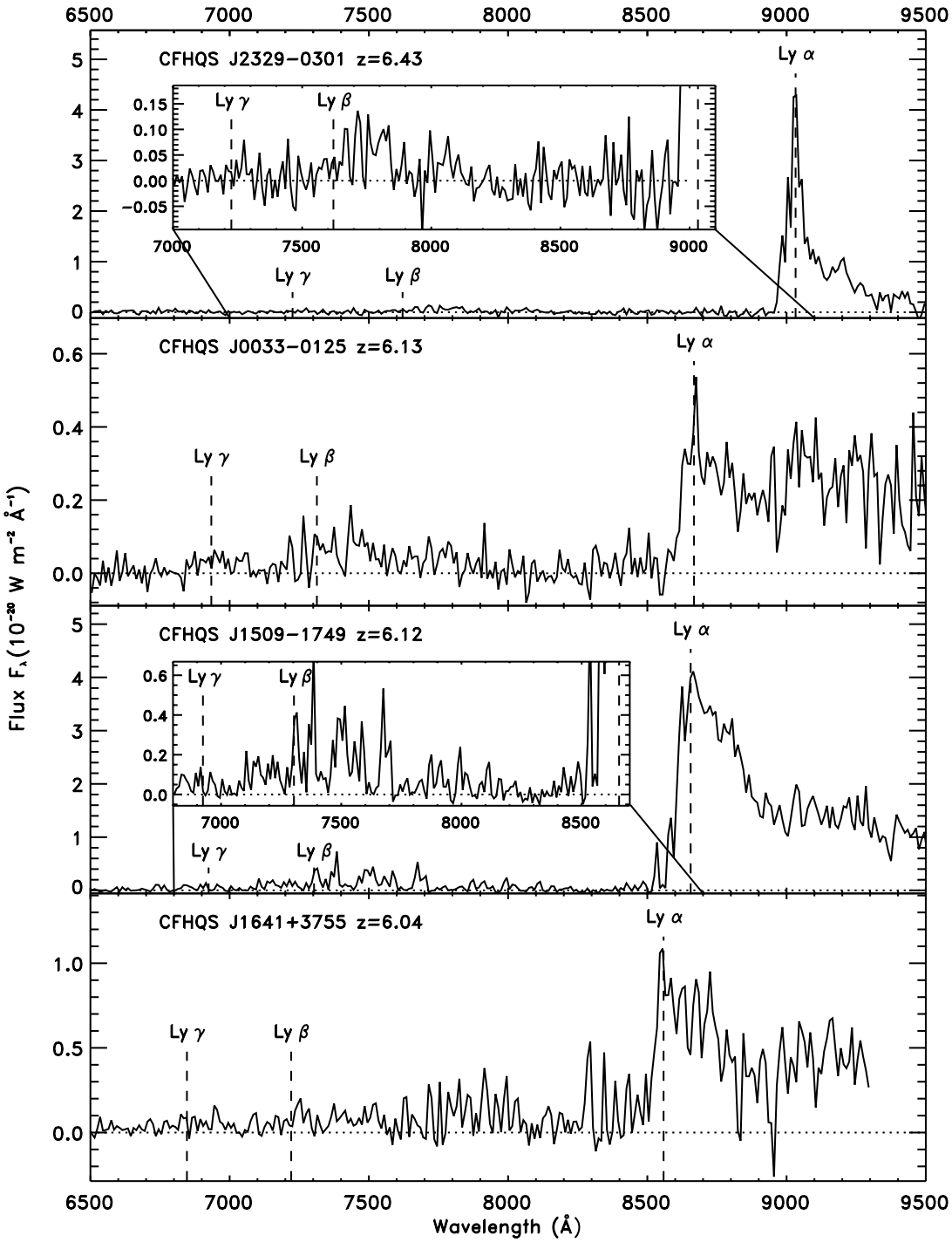

FIG. 3.—Optical spectra of the four newly discovered quasars. The expected locations of Lyα, Lyβ, and Lyγ are marked with dashed lines. The two quasars with the highest S/N spectra have inset panels which show the Lyα and Lyβ forests on an expanded scale. Note the huge variation in the strength and shape of the Lyα lines of the four quasars. All spectra are binned in 10 Å pixels. The spectrum of CFHQS J1641+3755 is contaminated by night-sky residuals at $\lambda > 7600$ Å.

All of the quasars except CFHQS J0033−0125 have strong Lyα emission lines.

Note that the spectra have a wide range of S/N due to the spread of 2 mag in brightness and different telescopes and exposure times used. Therefore, we leave a detailed discussion of the spectra to individual sections about each quasar in § 3.

Near-infrared spectroscopy of CFHQS J1509−1749 was performed using the Gemini Near Infrared Spectrograph (GNIRS; Elias et al. 2006) at Gemini South on 2006 March 14. Conditions were photometric with 0.8″ seeing. GNIRS was used in the cross-dispersed mode with the 32 line mm^{-1} grating and the short camera. With a 0.675″ wide slit, this setup gives the full near-IR spectrum from 0.8 to 2.4 μm at a constant resolution of $R = 900$. The total integration time of 3300 s was split into 11 equal exposures to enable background subtraction and cosmic-ray rejection.

The GNIRS spectrum was reduced with the IRAF Gemini package. The individual frames were flat-fielded and then background-subtracted using neighboring frames with the target shifted along the slit by 3″. The spectra were rectified, and then individual orders were extracted from the frames. The 11 individual frames

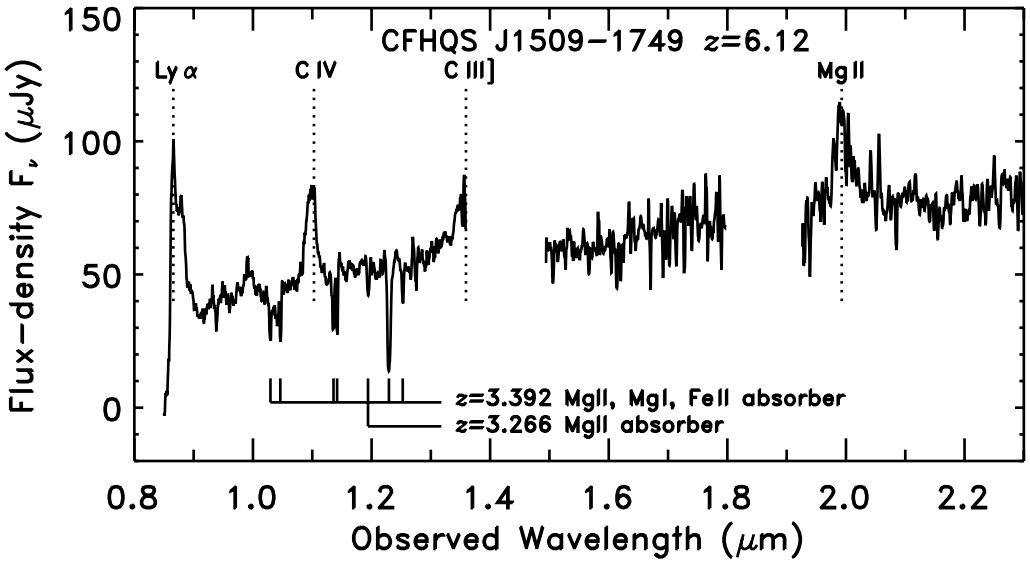

FIG. 4.—Near-IR spectrum of CFHQS J1509−1749 obtained with GNIRS. Several broad emission lines are labeled. Also shown are two metal-absorbing systems at $z = 3.266$ and 3.392. Note that this spectrum has been smoothed so the Mg II doublets, which are resolved in the original spectrum, appear as single lines.

for each order were then registered and combined using a bad-pixel mask and cosmic-ray rejection. Each order was wavelength-calibrated with the argon arc lamps. For orders 3–6, the wavelength calibration was refined using sky emission lines. The spectra were flux-calibrated using a spectrum of an A0-type standard star. One-dimensional spectra were extracted from each order and combined. Absolute flux calibration was achieved by passing the spectrum through the *J* filter response curve and normalizing to match the observed *J* magnitude. The near-IR spectrum of CFHQS J1509−1749 is shown in Figure 4 and discussed in § 3.

3. NOTES ON INDIVIDUAL QUASARS

3.1. *CFHQS J2329−0301*

The spectrum of this quasar shows a very high equivalent width Lyα emission line. The line has a strong narrow peak at $\lambda = 9029 \pm 2$ Å. The FWHM of this narrow peak is only 600 km s^{-1}. Taking this narrow peak to be the systemic redshift of the quasar (for reasons discussed below) would give a redshift of $z = 6.427 \pm 0.002$. This makes CFHQS J2329−0301 the most distant known quasar, surpassing SDSS J1148+5251 at $z = 6.419 \pm 0.001$ (Bertoldi et al. 2003b; Walter et al. 2003). The emission line has a broad base with a precipitous drop-off on the blue side at a Lyα redshift of $z = 6.37$. The spectral extent of the Lyα emission and transmitted flux in the Lyα forest will be discussed further in § 5.

We fit a power-law continuum curve by eye to the optical spectrum redward of Lyα (>9300 Å) by fixing the curve to the observed *J*-band flux density. Due to the low continuum level in this spectrum and relatively poor efficiency of GMOS at these wavelengths, the constraint on the power-law continuum slope is fairly poor, with spectral indices in the range $0.5 < \alpha_\nu < 1.5$ acceptable. Planned infrared spectroscopy should yield a better value for α_ν, and in this paper we adopt the "maximum continuum" case where $\alpha_\nu = 0.5$, as is typical for unreddened quasars.

With the continuum level defined as above, we measure the rest-frame equivalent width of the observed Lyα line to be 160 Å. The main uncertainty of this measurement is that from the continuum level. Since we have adopted the maximum continuum level, this gives a lower limit to the equivalent width. We also note that because of absorption of the Lyα line, the intrinsic equivalent width before absorption will be even higher. A rest-frame equivalent width of >160 Å for Lyα is very high compared with that measured for a composite spectrum of SDSS quasars of 93 Å (Vanden Berk et al. 2001). Another way of comparing the Lyα line to that of other quasars is the height of the peak of the line compared to the continuum. For CFHQS J2329−0301 the peak is 20 times the continuum level. This compares with a typical peak height of only 3 times the continuum level in the SDSS composite. All 19 quasars found at $z > 5.7$ in the SDSS have peaks less than 10 times the continuum level (Fan et al. 2006b). Therefore, it appears that CFHQS J2329−0301 has an unusually strong narrow component to its Lyα line. The high Lyα equivalent width explains the unusual location of this quasar in Figure 1 because Lyα falls in the z' filter.

If the peak of the Lyα line suffered from significant absorption, then the intrinsic peak would be even higher. We consider this unlikely given how high the Lyα peak and equivalent width are. Therefore, we are confident that the measured Lyα redshift of $z = 6.427 \pm 0.002$ is close to the systemic redshift of the quasar and adopt $z = 6.43 \pm 0.01$ as the redshift and its uncertainty. We plan to obtain spectroscopy of the Mg II emission line to compare with the Lyα redshift, since Mg II usually shows only small offsets from Lyα (Richards et al. 2002). We note that previous work on high-redshift quasars has usually defined the redshift via the Lyα peak (Fan et al. 2006a and references therein) and that the few high-redshift quasars with Lyα and Mg II redshifts show no systematic offset between them (Wyithe et al. 2005).

3.2. *CFHQS J0033−0125*

This is the faintest of the four quasars with $z' = 22.41$, which is close to the CFHQS magnitude limit of $z' = 22.5$. The spectrum therefore has low S/N. In contrast to CFHQS J2329−0301, CFHQS J0033−0125 has a very weak Lyα emission line which barely rises above the continuum. There is a narrow peak in Lyα at $\lambda = 8674$ Å, which we tentatively use to obtain the systemic redshift, giving $z = 6.13$, but the relatively low height of this peak above the continuum makes this redshift estimate quite uncertain. Plausible values for the redshift lie in the range $6.10 < z < 6.18$.

The equivalent width of the Lyα emission is difficult to measure due to the uncertain continuum, but it appears to be <10 Å. With the exception of this narrow peak, CFHQS J0033−0125 resembles the lineless quasars discovered in the SDSS (Fan et al. 2006a and references therein). We suspect that the low equivalent width of Lyα in this quasar is due to an unusually high number of dense pockets of neutral hydrogen close to the quasar.

Despite the low S/N, it is apparent that there is a higher transmitted flux in the Lyα forest at observed wavelengths 7500–8000 Å than at 8000–8500 Å. This is observed in other quasars at similar redshift (see, e.g., CFHQS J1509−1749 in the same figure), as expected based on the increase of the Lyα forest density with redshift, and provides confidence that this object really is a $z > 6$ quasar and not an unusual broad absorption line quasar such as have been found in the SDSS (Hall et al. 2002).

3.3. *CFHQS J1509−1749*

This quasar is the brightest discovered so far in the CFHQS, with $z' = 20.26$. This magnitude is similar to the faintest $z \sim 6$ SDSS quasars. The optical spectrum is the most sensitive of the four presented here, resulting in the highest S/N. The spectrum shows a strong continuum break across the broad Lyα emission line. This line has a peak at about 8660 Å ($z = 6.12$) but is highly asymmetric, with considerably more flux on the red side of this peak than the blue side due to neutral hydrogen absorption. The Lyα emission line has a rest-frame equivalent width of 48 Å, which is typical of high-redshift quasars (unlike CFHQS J0033−0125 and CFHQS J2329−0301). A more detailed discussion of this optical spectrum is given in § 5.

The near-infrared spectrum of CFHQS J1509−1749 is shown in Figure 4. The gaps at 1.4 and 1.9 μm are due to opaque wavelength regions of the Earth's atmosphere. Emission lines of Lyα, C IV, C III], and Mg II are visible, along with some weaker lines. Also evident are strong absorption lines in the *J* band, which are discussed in more detail below.

The Mg II emission line is a low-ionization line that shows significantly less asymmetry and blueshift (relative to the narrow [O III] line) than high-ionization lines such as C IV (Richards et al. 2002). Therefore, it provides the best indicator of the systemic redshift of a quasar at a redshift too high for any narrow lines to be observable. We have performed a Gaussian fit to the Mg II line profile assuming an underlying power-law continuum. Although it is known that the continuum around Mg II is not flat due to many blended weak Fe II lines, this does not affect the determination of the peak wavelength of a fitted Gaussian. The peak of the Gaussian for Mg II is at 1.9923 ± 0.0015 μm, giving a redshift of $z = 6.118 \pm 0.006$. We hereafter refer to the redshift as $z = 6.12$. Note that this redshift agrees with the peak of Lyα in both the GMOS and GNIRS spectra. The C IV line is substantially offset from the Mg II and Lyα peaks. The measured C IV peak is at 1.0982 ± 0.0010 μm, which is a blueshift from Mg II of 1200 km s^{-1}. Blueshifts of this size are common among lower redshift quasars (Richards et al. 2002).

3.3.1. *Absorption Lines*

Despite the moderate S/N ratio ($\sim$10) of the near-infrared spectrum of CFHQS J1509−1749, two strong absorption systems of low ionization are clearly detected at $z = 3.266 \pm 0.001$ and 3.392 ± 0.001. The spectral resolution is $R \simeq 900$; thus, the two Mg II doublets are well resolved. They also are fully saturated, as both lines of each doublet have roughly the same equivalent width: $w_{\rm obs}(2796, 2803) = 5.0$ and 21.0 Å for the $z = 3.266$ and 3.392 systems, respectively. The 3 σ equivalent width detection limit in the *J* band is $w_{\rm obs,lim} = 4.0$ Å; thus, even the weaker Mg II system is well detected, at about the 4 σ level.

The $z = 3.392$ system is extremely strong, $w_{\rm rest}(2796) = 4.8$ Å, with associated absorptions from the Mg I singlet [$w_{\rm rest}(2852) = 1.5$ Å] and Fe II lines [2344, 2382, 2586, and 2600 Å; $w_{\rm rest}(2600) = 2.9$ Å]. This set of absorption lines is characteristic of damped Lyα absorbers (DLAs): about 80% of the Mg II systems with $w_{\rm rest}(2796) > 1.0$ Å are DLAs (Rao et al. 2006), and moreover, all systems with $w_{\rm rest}(2852) > 0.7$ Å are DLAs (Rao & Turnshek 2000). This system has all the characteristics of a DLA. The $z = 3.266$ system has an Mg II doublet with $w_{\rm rest}(2796) = 1.2$ Å, but no other absorption lines are detected.

The Mg II doublet is detectable in this spectrum over the redshift range $2.10 \leq z \leq 3.83$. This yields an incidence of $w_{\rm rest}(2796) > 1.0$ Å systems of $dN/dz \simeq 1.2$ for this single line of sight. This value of dN/dz is 3 times greater than the results from Mg II absorption studies at $z \sim 2$, which give $dN/dz = 0.40 \pm 0.05$ for $w_{\rm rest}(2796) > 1$ Å systems (Nestor et al. 2005; Prochter et al. 2006). Given the high Poisson noise, we cannot say that there is a statistically significant excess in absorption toward CFHQS J1509−1749. We do not expect significant cosmic evolution of dN/dz for strong Mg II absorbers from $z = 2$ to 3.4, because only a weak evolution, if any, is observed at $1.0 < z < 2.3$. Therefore, the apparent excess toward this quasar, if significant, must be due to a different cause, perhaps related to the higher quasar redshift.

To determine if this discrepancy is statistically significant, one can use the published results of Keck ESI spectra of $z \sim 6$ SDSS quasars. Strong Mg II doublets are detected toward SDSS J1044−0125 at $z = 2.2786$ and SDSS J1306+0356 at $z = 2.20$ and 2.53, while there is no Mg II absorption toward SDSS J0836+0054, SDSS J1030+0524, and SDSS J1148+5251 (Becker et al. 2001; Djorgovski et al. 2001; Fan et al. 2003; White et al. 2003; Ryan-Weber et al. 2006). The two Mg II systems of highest z have clear, associated Fe II (2586 and 2600 Å) strong absorption, as could be seen from the quasar spectra, although this is not mentioned by the authors. No equivalent width is reported for any of the Mg II lines, but $w_{\rm obs}(2796)$ should be of order 5 Å or higher for the three systems. The sum of the redshift ranges for each quasar over which strong Mg II absorption is detectable is $\Delta z = 2.79$, which yields $dN/dz \simeq 1.08$. A similar value is obtained when adding the two systems toward CFHQS J1509−1749 to the sample, $dN/dz \simeq 1.11$ (or $0.61 < dN/dz < 1.60$ at the 1 σ level). Thus, we see tentative evidence for an enhancement in the absorber incidence for the most distant quasars.

One possible explanation for this is that some of the most luminous $z \sim 6$ quasars are gravitationally lensed (Wyithe & Loeb 2002; Comerford et al. 2002). The high incidence of Mg II absorption would then be related to above average mass density along the line of sight. However, searches for multiple images and lensing galaxies in the highest redshift SDSS quasars do not show any evidence for lensing (Fan et al. 2003; Richards et al. 2004; Willott et al. 2005b). There is no evidence for multiple images from the ground-based imaging of the CFHQS quasars discovered so far (Fig. 2).

3.3.2. *Dust Reddening*

The full near-IR coverage of the GNIRS spectrum allows one to investigate the continuum shape of this quasar. A power-law fit to the *J*-band continuum gives a spectral index of $\alpha_\nu = 1.00 \pm 0.02$. This is considerably redder than typical quasars, which have $\alpha_\nu = 0.5$ (Richards et al. 2003). However, inspection of the *H*- and *K*-band spectra show that the spectrum flattens here.

Because of the complex shape of quasar spectra at $\lambda_{\rm rest} > 2300$ Å due to blended Fe II lines and Balmer continuum (the

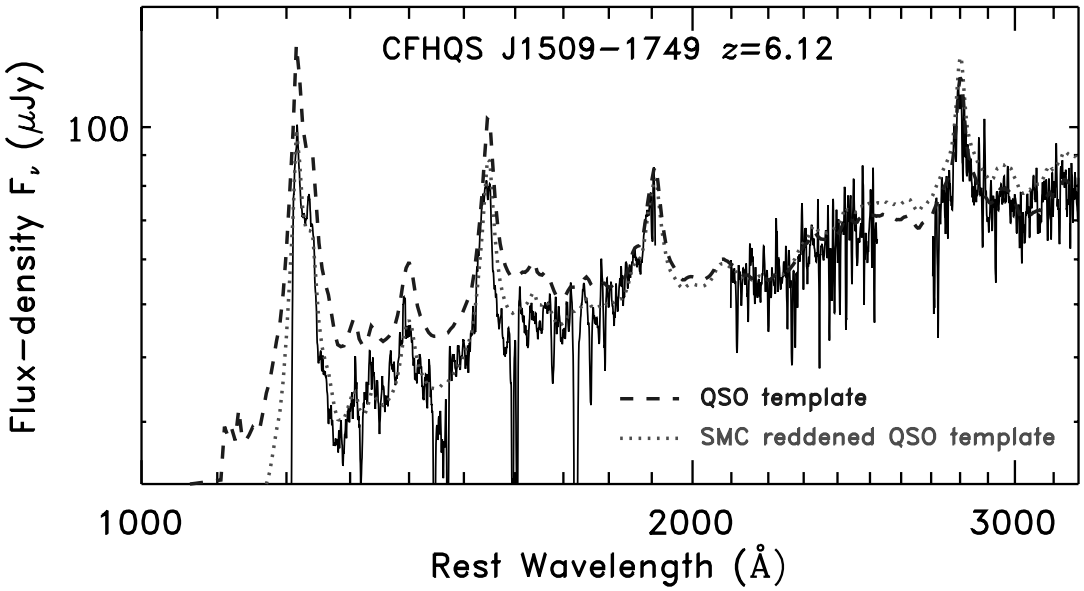

FIG. 5.—Rest-frame UV spectrum of CFHQS J1509−1749 plotted on a log-log scale. At $\lambda_{\rm rest} > 2000$ Å the spectrum is well fit by an unreddened quasar template (*blue dashed line*), but at $\lambda_{\rm rest} < 2000$ Å the spectrum is considerably reddened and can be fit by a quasar template reddened by SMC dust (*red dotted line*). Note that this SMC-dust-reddened quasar overpredicts the flux at $\lambda_{\rm rest} > 2500$ Å. [*See the electronic edition of the Journal for a color version of this figure.*]

"small blue bump"), we do not fit a power law to these data but instead overplot a composite quasar spectrum constructed from spectra of SDSS quasars (Fig. 5). This shows that a typical quasar spectrum fits the continuum well in the *H* and *K* bands but not at shorter wavelengths ($\lambda_{\rm rest} < 2000$ Å). An analysis of extinction curves of reddened SDSS quasars (Hopkins et al. 2004) has shown that quasar dust is most often similar to the dust in the Small Magellanic Cloud (SMC). This extinction curve steepens significantly in the UV compared to that of typical Milky Way (MW) dust. We also plot in Figure 5 the composite quasar spectrum reddened by enough SMC-type dust ($A_V = 0.10$) to match the *J*-band spectrum. Although this reddened quasar template fits well at <2000 Å, it predicts a steeper slope at >2000 Å than is observed. We observe essentially no reddening of the intrinsic quasar slope over the range 2000–3200 Å. We have checked the possibility of reddening by dust with known extinction laws (e.g., MW, LMC, and SMC) in the $z \sim 3$ absorbers and found fits no better than SMC dust at the quasar redshift.

One possible explanation for the sharp change in extinction at $\lambda_{\rm rest} \approx 2000$ Å is that the dust reddening this quasar has been created by Type II supernovae. In our galaxy the dominant dust production mechanism is low-mass AGB stars (Gehrz 1989). But at $z > 6$ there is insufficient time (<1 Gyr) for such stars to have evolved off the main sequence. Therefore, core-collapse supernovae (whose progenitors have short main-sequence lifetimes) may be the main dust producers in the early universe. The heavy-metal content of supernova explosions is expected to produce vast quantities of dust with a quite different composition and grain size distribution from that from AGB stars (Todini & Ferrara 2001). Recent observations of a $z > 6$ broad absorption line quasar and a $z > 6$ gamma-ray burst have both shown signs of extinction curves which are similar to that inferred here (Maiolino et al. 2004; Stratta et al. 2007). However, without rest-frame optical observations, it is impossible to say if this is due to supernovae dust (which would have considerable, but constant, extinction at 2000–3000 Å; Maiolino et al. 2004) or dust with only very small grains (so no extinction at all at >2000 Å).

We conclude that CFHQS J1509−1749 shows unusual dust reddening. Infrared observations probing the rest-frame optical are necessary to determine if this dust matches the predicted extinction curve of dust created by Type II supernovae.

3.4. *CFHQS J1641+3755*

The optical spectrum of this quasar (Fig. 3) shows a broad Lyα line with a sharp drop in flux on the blue side. The Lyα line has typical asymmetry, with the peak close to the sharp drop. We assume the peak at $\lambda = 8555$ Å defines the systemic redshift of $z = 6.04$. The redshift uncertainty is ± 0.04. The spectrum of CFHQS J1641+3755 is affected by night-sky subtraction residuals caused by incomplete removal of fringing, which lead to excess positive flux. This explains the apparent high transmission of the Lyα forest for this quasar. Because of this we cannot with certainty define the continuum level of this quasar redward of Lyα. Given the fact that the quasar has a $z' - J$ color typical of quasars (Fig. 1), we assume a spectral index of $\alpha_\nu = 0.5$ to calculate the absolute magnitude from the *J*-band magnitude.

4. MULTIWAVELENGTH DATA

We have searched the NASA/IPAC Extragalactic Database (NED) at the locations of the four new quasars and found no coincident objects from any other survey. Two of the quasars, CFHQS J0033−0125 and CFHQS J1641+3755, are located in regions of the FIRST radio survey (Becker et al. 1995). We have checked the FIRST image cutouts, and neither quasar is detected to a flux limit of ≈0.5 mJy, meaning that neither quasar is radio-loud.

4.1. 1.2 mm *MAMBO Observations: Dust and Ultraluminous IR Starbursts*

Follow-up observations of large samples of $2 \lesssim z \lesssim 6$ quasars at millimeter and submillimeter wavelengths have shown that a large fraction (30%) of optically luminous quasars are hyperluminous infrared ($L_{\rm FIR} \gtrsim 10^{13}\ L_\odot$) sources. In these sources the far-IR luminosity is mainly related to the warm (40–60 K) dust, with estimated dust masses of a few $10^8\ M_\odot$. The heating of the warm dust appears to be dominated by the starburst

activity of the quasar host galaxy, and the implied star formation rates are $\sim$1000 $M_\odot$ yr^{-1} (e.g., Omont et al. 2001, 2003). In a growing number of cases, warm and dense molecular gas is detected via CO emission lines, and in a few cases via other species, revealing the presence of large reservoirs of molecular gas, the fuel of the star-forming activity (see reviews by Cox et al. 2005; Solomon & Vanden Bout 2005). The presence of such huge starbursts in phases of strong accretion of the quasars proves the simultaneity of major phases of growth of the most massive (elliptical) galaxies and their supermassive black holes, and is an important clue for explaining the black hole–spheroid relation.

The detection of millimeter or submillimeter dust emission has been reported in eight $z > 5.7$ SDSS quasars (but only three at $z \geq 6$) with typical flux densities at 1.2 mm of a few millijanskys (Bertoldi et al. 2003a; Priddey et al. 2003; Robson et al. 2004; Beelen et al. 2006; Wang et al. 2007). Their properties and detection rate, as well as the CO detection in J1148+5251 (Bertoldi et al. 2003b; Walter et al. 2003, 2004), are comparable to other high-z strong starburst quasars. This shows the presence of giant starbursts and vast amounts of molecular gas, with heavy elements, less than 1 billion years after the big bang. J1148+5251 is also the first high-z source where [C II] line emission has been detected (Maiolino et al. 2005).

It is important to extend the exploration of the millimeter properties and star formation to a larger sample of $z \gtrsim 6$ quasars, especially among the more numerous, fainter quasars in the CFHQS. A crucial question for building up the black hole–spheroid relation is whether the 1.2 mm emission, and hence the star formation rate, are strongly dependent on the UV luminosity, or only weakly as at $2 < z < 4$ (Beelen 2004; Cox et al. 2005; Wang et al. 2007). Therefore, we have observed at 1.2 mm the four $z > 6$ CFHQS quasars.

The observations were performed within the pool observing sessions at the IRAM 30 m telescope in the winter of 2006/2007, using the 116 element version of the Max Planck Millimeter Bolometer (MAMBO) array (Kreysa et al. 1998) operating at a wavelength of 1.2 mm (250 GHz). We used the standard on-off photometry observing mode, chopping between the target and sky at 2 Hz, and nodding the telescope every 10 or 20 s (see, e.g., Wang et al. 2007). On average, the noise of the channel used for point-source observations was about $(35–40)t^{-1/2}$ mJy beam^{-1} (where t is the integration time in seconds). This allowed us to achieve an rms $\lesssim$0.5 mJy for each of the four sources, with about 1.5 hr of telescope time per source. The data were reduced with standard procedures to minimize the sky noise with the MOPSIC package developed by R. Zylka.

The results are shown in Table 3. There is no strong source with a flux significantly larger than 1 mJy. CFHQS J0033−0125 is detected at S/N > 3 with flux 1.13 ± 0.36 mJy. In addition, CFHQS J1509−1749 has a very marginal (S/N ~ 2) detection. The mean flux in the four sources is 0.56 ± 0.23 mJy. This is an order of magnitude weaker than J1148+5251. It corresponds nevertheless to a far-infrared luminosity $\gtrsim 10^{12}\ L_\odot$ and a star formation rate of $\sim$300 $M_\odot$ yr^{-1}, typical of ultraluminous infrared galaxies. This mean 1.2 mm flux for our four CFHQS sources is significantly smaller than the mean value that one can deduce from Tables 1 and 2 of Wang et al. (2007) for 17 $z \sim 6$ SDSS quasars, which is $\approx$1.3 mJy. This difference could be related to the fainter UV luminosity of the CFHQS quasars. Observations of more CFHQS quasars in the future will allow tighter constraints on the luminosity dependence of far-infrared emission in the most distant quasars.

TABLE 3
MAMBO 1.2 mm Photometry of CFHQS Quasars

Quasar	Redshift	$S_{1.2}$ (mJy)
CFHQS J0033−0125	6.13	1.13 ± 0.36
CFHQS J1509−1749	6.12	1.00 ± 0.46
CFHQS J1641+3755	6.04	0.08 ± 0.46
CFHQS J2329−0301	6.43	0.01 ± 0.50

5. IONIZATION STATE OF THE $z > 5$ IGM

The spectra of the quasars presented here are discovery spectra. They generally have modest integration times. Considering the faintness of most of these quasars, detailed analysis of the implications of these quasars for cosmic reionization is deferred until we have higher S/N and resolution spectroscopy. In this section we describe the information we can get from our observations on the ionization state of the high-redshift universe. We only discuss the highest redshift quasar, CFHQS J2329−0301, and the brightest quasar, CFHQS J1509−1749, since the other two quasars have very low S/N spectra. In addition, the systemic redshifts of CFHQS J0033−0125 and CFHQS J1641+3755 are poorly determined due to the lack of near-IR spectroscopy and low S/N of broad Lyα. We note that poor sky subtraction can be a serious problem for studies of the high-redshift IGM. The spectra we use in this section are from GMOS in the nod-and-shuffle mode, which is well documented to provide excellent sky subtraction (Abraham et al. 2004).

5.1. *Intrinsic Quasar Spectra*

In order to determine the neutral hydrogen absorption in these quasar spectra, we first need to determine the intrinsic spectra before absorption. This is not a trivial task given the large amount of absorption shortward of and around the Lyα emission line. As described in § 3, we used optical/near-IR spectroscopy and/or photometry to determine the continuum power-law indices at $\lambda_{\rm rest} > 1250$ Å. CFHQS J1509−1749 has $\alpha_\nu = 1.0$. The continuum for CFHQS J2329−0301 is not well defined, so we adopt $\alpha_\nu = 0.5$. Observations of a large sample of quasars at lower redshift show a continuum break in the region 1200 Å $< \lambda <$ 1300 Å, with a steeper power-law index of $\alpha_\nu = 1.7$ at shorter wavelengths (Telfer et al. 2002). Therefore, we adopt $\alpha_\nu = 1.7$ for both quasars at $\lambda_{\rm rest} < 1250$ Å.

Because we are interested in absorption close to the quasar, we also include broad emission lines of Lyβ, Lyα and N v. For CFHQS J1509−1749 we set the width of these lines in velocity to be equal to the measured C IV FWHM $= 5600$ km s^{-1} (consistent with the Mg II FWHM). The peak height of the Lyα line is determined by eye, and the Lyβ and N v lines have the same fraction of the Lyα peak height as in the composite spectrum of Telfer et al. (2002). For CFHQS J2329−0301 the intrinsic width of the Lyα emission line is very uncertain. The spectrum shown in Figure 3 has a strong narrow Lyα line on top of a broad base. Whether this observed profile is due to absorption of a single broad line or a combination of broad+narrow lines is uncertain. We do not currently have near-IR spectroscopy for the measurement of other broad line widths. We adopt a single Gaussian line with a width of FWHM $= 3400$ km s^{-1} and peak equal to the observed Lyα peak. The emission lines only have a significant effect very close to the quasar redshift, so this uncertainty does not affect the results presented.

TABLE 4
IGM Absorption in Bins of Width $\Delta z = 0.15$ toward the $z = 6.12$ Quasar CFHQS J1509−1749

Redshift	Transition	Transmission	$\tau_{\mathrm{Ly}\alpha}$
5.225.....	Lyα	0.110 ± 0.004	2.20
5.375.....	Lyα	0.084 ± 0.005	2.48
5.525.....	Lyα	0.051 ± 0.005	2.97
5.675.....	Lyα	0.026 ± 0.005	3.64
5.825[a].....	Lyα	0.000 ± 0.005	>4.64
5.825[b].....	Lyβ	0.097 ± 0.022	5.25

[a] Optical depth is a 2 σ lower limit.
[b] Transmission is after correction for foreground Lyα as described in the text, and the optical depth is the equivalent Lyα optical depth using $\tau_{\mathrm{Ly}\alpha} = 2.25\tau_{\mathrm{Ly}\beta}$.

5.2. *IGM Optical Depth*

The observed quasar spectra are divided by their intrinsic spectra as defined in § 5.1 to determine the transmission as a function of wavelength. The transmission is then used to calculate the effective optical depth. When binning over multiple pixels, each pixel is weighted by the inverse variance to reduce the effects of noise spikes due to bright-sky emission lines. For CFHQS J2329−0301 it is evident that the low S/N of this discovery spectrum prevents us from placing strong constraints on the optical depth of the IGM along this line of sight. We detect flux in the region of Lyα absorption at $z < 5.75$, but not at higher redshifts. In a large bin covering the redshift range $5.35 < z < 5.75$ we measure a Lyα optical depth of $\tau = 2.67 \pm 0.17$. In the higher redshift bin of $5.75 < z < 6.35$ we obtain only a 2 σ limit on the optical depth of $\tau > 3.93$. This lower limit for the optical depth is considerably lower than the detections and limits for $z > 6.2$ SDSS quasars, so we do not discuss it further in this paper and await higher S/N spectroscopy.

The spectrum of CFHQS J1509−1749 does have high enough S/N to investigate the optical depth of the IGM. We bin the spectrum in intervals of $\Delta z = 0.15$ to get the effective optical depth along this line of sight. We ensured that the highest redshift bin does not include flux that may be associated with the quasar proximity zone discussed in § 5.3. Values of the Lyα transmission and effective optical depth are given in Table 4. The uncertainties reflect only the photon noise, which is the dominant cause of measurement uncertainty. However, in most cases this uncertainty is lower than the intrinsic cosmic variance (Fan et al. 2006b).

The Lyβ transmission is measured only for the highest redshift bin. Lower redshift bins of Lyβ would overlap with the higher order Lyman transitions. The Lyβ region at $z = 5.8$ is contaminated by foreground Lyα absorption at $z = 4.7$. This foreground Lyα absorption is corrected for statistically using the curve of effective Lyα optical depth against redshift measured for a large number of lines of sight at $z < 5.5$. Fan et al. (2006b) quote this as $\tau_{\mathrm{Ly}\alpha} = 0.85[(1+z)/5]^{4.3}$. Applying this correction gives a value for the Lyβ transmission of 0.097 ± 0.022. The quoted uncertainty does not include the uncertainty in the foreground Lyα transmission. For this bin we detect zero flux in Lyα, but there is a >4 σ detection of flux in Lyβ. This is because the oscillator strength for the Lyβ transition is considerably lower than for Lyα.

Figure 6 plots transmission against redshift for the five Lyα bins and one Lyβ bin. Also plotted are Lyα transmissions for SDSS quasars in Fan et al. (2006b). The solid curve is an extrapolation of the fit to $z < 5.5$ quasars described above. This curve

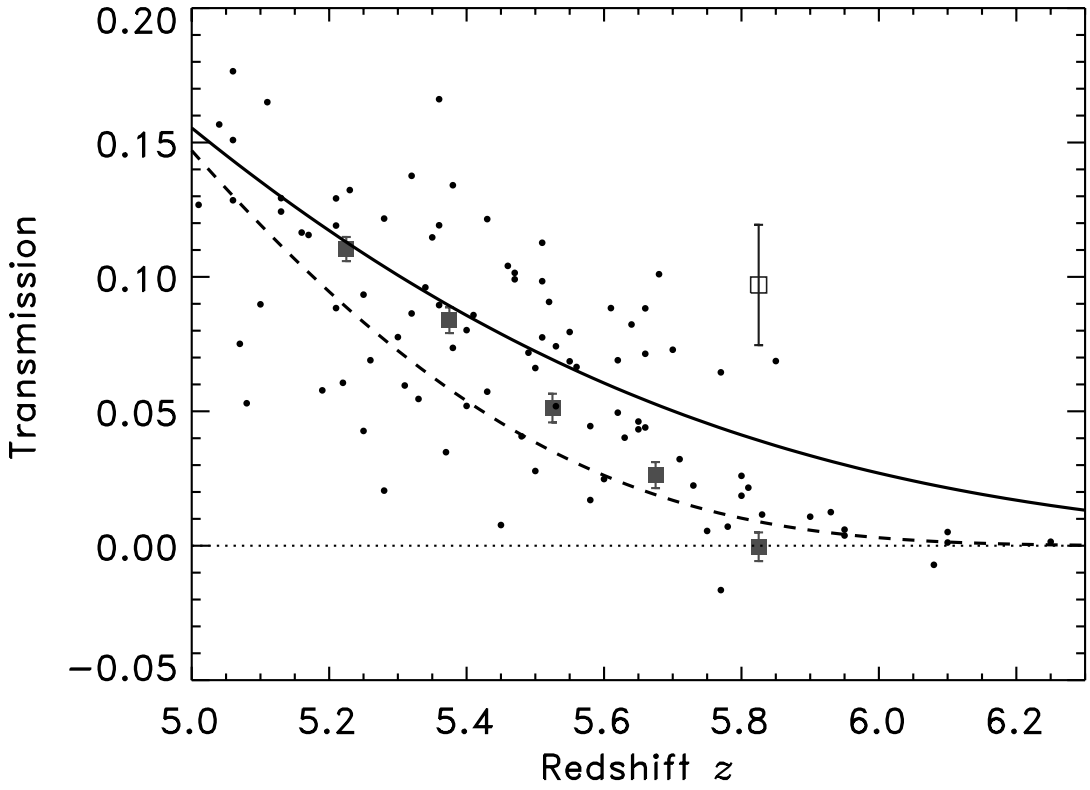

Fig. 6.—Lyman transmission in the spectrum of CFHQS J1509−1749. The filled red squares show the Lyα transmission, and the open blue square is the Lyβ transmission in bins of width $\Delta z = 0.15$. The small circles show the Lyα transmission from the sample of 19 SDSS quasars of Fan et al. (2006b). The solid line is the fit to the Lyα transmission of $z < 5.5$ quasars given by Fan et al. (2006b). The dashed line was obtained by Becker et al. (2007) by fitting flux PDFs of $z < 5.4$ quasars with a lognormal optical depth distribution. At $z > 5.7$ our data (and most of those in the SDSS) fall below the extrapolation of the Fan et al. curve. [*See the electronic edition of the Journal for a color version of this figure.*]

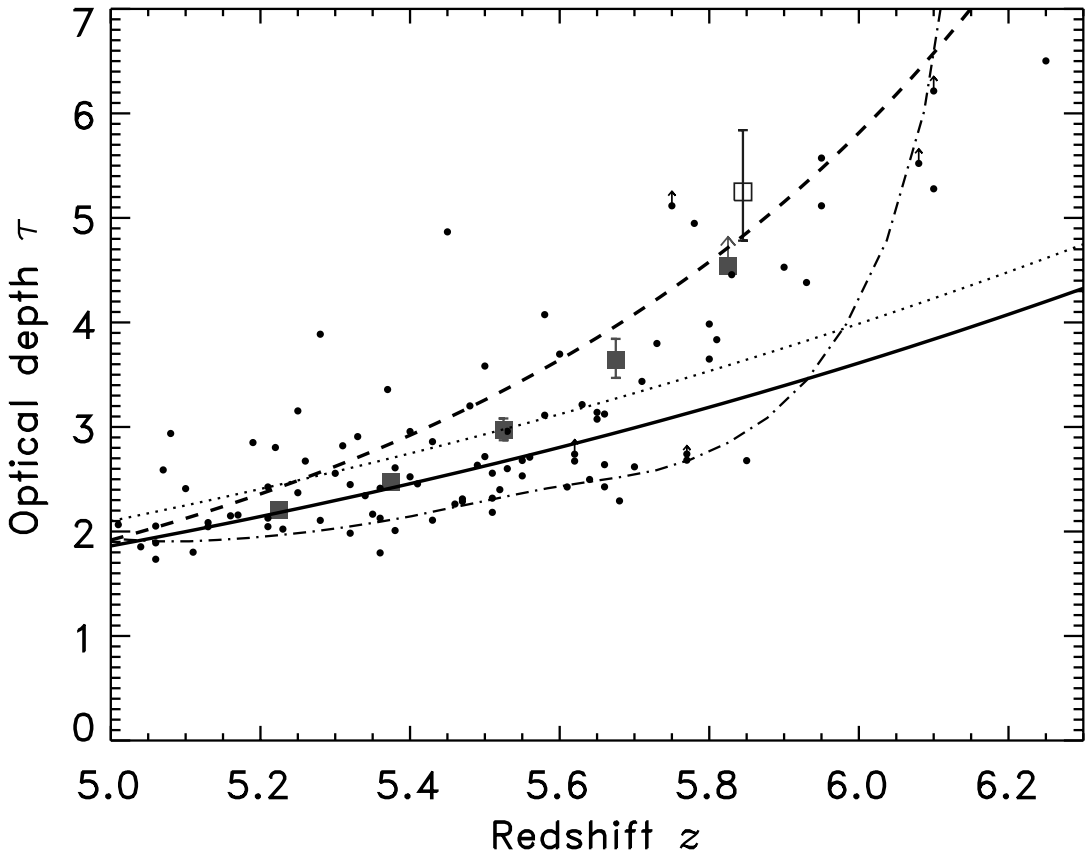

FIG. 7.—Effective Gunn-Peterson optical depth from the spectrum of CFHQS J1509−1749 (symbols are as in Fig. 6). The Lyβ point (*open blue square*) is the equivalent Lyα optical depth. The solid and dashed lines are the extrapolations from lower redshift quasars by Fan et al. (2006b) and Becker et al. (2007) (as in Fig. 6). The dotted and dot-dashed lines are the effective optical depth evolution in the simulations of Paschos & Norman (2005) and Gnedin & Fan (2006), respectively. [*See the electronic edition of the Journal for a color version of this figure.*]

is consistent with the increasing absorption at higher redshifts being solely due to the increase in number density of Lyα forest clouds for typical model IGM parameters (Miralda-Escudé et al. 2000; see also the model curves in Fig. 7). The Lyα data for CFHQS J1509−1749 lie close to the curve at $z < 5.4$ but fall well below it at higher redshifts, indicating a sharp evolution in the hydrogen neutral fraction compared to the expected extrapolation.

Becker et al. (2007) have cast doubt on this form for the expected evolution in transmission. They showed that the Lyα transmitted flux probability distributions of quasars at $2 < z < 5$ are better fit by lognormal optical depth distributions than the distributions from theoretical models such as that of Miralda-Escudé et al. (2000). Because the transmitted flux for the highest redshift quasars primarily depends on the low optical depth tail of the distribution in voids, using the correct form for the optical depth distribution is important. The dashed curve in Figure 6 shows the expected transmission evolution based on fits to quasars at $z < 5.4$ by Becker et al. It is clear that this curve falls much more rapidly than that of Fan et al. (2006b) and is consistent with the $z > 5.8$ data for no evolution in the hydrogen neutral fraction. However, the Becker et al. curve does not do a good job of fitting the data at $5.4 < z < 5.7$, where it predicts transmission considerably lower than most of the SDSS data points. It is beyond the scope of this paper to investigate the cause of this discrepancy, but we note that Becker et al. used linear fits to evolution parameters, so it is perhaps not surprising that this linear fit cannot accommodate the data at all redshifts.

Figure 7 shows the optical depth evolution. For the highest redshift bin, the Lyα point is a 2 σ lower limit. For the Lyβ point, we plot the equivalent Lyα optical depth assuming $\tau_{\mathrm{Ly}\alpha} = 2.25\tau_{\mathrm{Ly}\beta}$ (Fan et al. 2006b; Gnedin & Fan 2006). The Lyα limit is consistent with the Lyβ detection. The line of sight to CFHQS J1509−1749 shows one of the highest optical depth measurements at $z \approx 5.8$. As for the previous plot, it is clear that there is a sharp evolution away from the Fan et al. (2006b) low-redshift curve at $z > 5.4$. Assuming standard IGM parameters (e.g., Fan et al. 2001), the optical depth evolution for CFHQS J1509−1749 is consistent with an increase in the IGM hydrogen neutral fraction by a factor of 3 from $z = 5$ to 6.

Also plotted in Figure 7 are two simulation results for the Gunn-Peterson optical depth evolution. The simulations of Paschos & Norman (2005; Fig. 7, *dotted curve*) show no evolution away from the low-redshift extrapolation in this redshift range, because reionization is 99% complete by $z = 6.4$. Our data and those of the SDSS clearly show that the optical depth is greater than in this model at $z > 5.7$.

The dot-dashed curve is the optical depth evolution for the L8N256 simulation of Gnedin & Fan (2006). In these simulations the overlap period of reionization occurs at $z = 6.2$. The emissivity at $z = 6 \pm 0.1$ in this model is set to match the SDSS observations, so we should expect agreement at this redshift. This simulation predicts a very sharp increase in the optical depth at $z > 6$. As is evident from Figure 7, the actual evolution for CFHQS J1509−1749 and SDSS quasars is somewhat more gradual than in this model. This suggests that the period of overlap is likely more extended than in the simple model. As highlighted by Gnedin & Fan (2006), the optical depth at the end of overlap is dominated by Lyman limit systems, and simulations need to both

resolve very small scales and cover very large scales. Both simulations give τ-evolution during the epoch in which reionization is complete that is comparable to the Fan et al. (2006b) curve and much flatter than the Becker et al. (2007) curve. We defer a more detailed comparison of the observed optical depth evolution with models until we have high-S/N spectra of more CFHQS quasars.

5.3. *Highly Ionized Near-Zones*

One of the difficulties of probing the neutral hydrogen fraction via quasar spectroscopy is that Lyman series absorption is extremely efficient. Because the density of the IGM increases at high redshifts, a neutral fraction (by volume) of only 2×10^{-4} at $z = 6$ gives an optical depth at Lyα of $\tau \sim 5$ (e.g., Fan et al. 2006b).

Therefore, it is useful to identify methods which are more sensitive to high neutral fractions. One of these which has been extensively studied in recent years is using the size of the region around the quasar which it has ionized. This is variously referred to as an HII region, Stromgren sphere, or highly ionized near-zone. We adopt the term near-zone as this does not imply that the surroundings are significantly neutral.

For a quasar embedded in a uniform-density IGM, the size of the ionization front from the quasar is proportional to $f_{\rm H\,I}^{-1/3}$, $\dot{N}^{1/3}$, and $t_Q^{1/3}$, where $f_{\rm H\,I}$ is the fraction of hydrogen in the IGM that is neutral, $\dot{N}$ is the number of ionizing photons emitted by the quasar per second, and t_Q is the age of the quasar activity (Cen & Haiman 2000; Wyithe & Loeb 2004). Note that the latter two terms could be combined into the total number of ionizing photons emitted so far by the quasar. Therefore, a measurement of the size of the ionization front (from spectroscopy) combined with knowledge of the number of ionizing photons emitted would give the neutral fraction.

This method has been employed to argue that the highest redshift SDSS quasars are embedded in a highly neutral IGM ($f_{\rm H\,I} \gtrsim 0.1$; Wyithe & Loeb 2004; Wyithe et al. 2005; Mesinger & Haiman 2007). However, there are many complicating factors, such as the uncertain density distribution close to luminous quasars and preionization by associated galaxies (Yu & Lu 2005). Uncertainty in the systemic redshifts can also be an issue, leading to a typical uncertainty in the near-zone size of $\approx$1 Mpc for redshifts from the Lyα line.

An additional uncertainty comes from relating observations to simulations. Defining the exact end of a near-zone from spectra is difficult. This is especially true for $5.7 < z < 6.2$ quasars, which typically do not show Gunn-Peterson troughs immediately shortward of their near-zones. In order to be able to define near-zone sizes for a wide range of spectra, Fan et al. (2006b) adopted the definition as the point in the spectra where the Lyα transmission first drops to $T < 0.1$ for spectra binned in 20 Å pixels. Most studies involving just those quasars at the upper end of the SDSS redshift distribution (e.g., Wyithe et al. 2005; Yu & Lu 2005) define the near-zone size as corresponding to the onset of the Gunn-Peterson trough (typically $T \lesssim 0.01$). Bolton & Haehnelt (2007a) discuss many of the uncertainties associated with using near-zone sizes to estimate $f_{\rm H\,I}$. Chief among these is the fact that the observed size may not correspond to the actual size of the ionized region due to significant residual neutral hydrogen left behind the ionization front.

As mentioned previously, the sizes of near-zones are expected to be related to the quasar luminosity. For the classical case of an expanding H II region, the near-zone size is proportional to $\dot{N}^{1/3}$. Bolton & Haehnelt (2007a) found the expected dependence to be $\dot{N}^{1/2}$ for near-zones defined as $T < 0.1$. The CFHQS magnitude limit is 2.3 mag fainter than that of the SDSS, meaning that the CFHQS quasars are on average almost a factor of 10 lower in luminosity. Therefore, the CFHQS near-zone sizes are expected to be between 2 and 3 times smaller than those in the SDSS. Comparing the near-zones sizes for the final CFHQS sample to the final SDSS sample will allow a test of the luminosity dependence.

In the top and middle panels of Figure 8 we show the transmission in the spectrum of CFHQS J1509−1749 close to the quasar redshift. The middle panel shows the Lyα and Lyβ transmission in 20 Å bins. It is seen that the Lyα transmission first drops below $T = 0.1$ at a distance of 4.3 Mpc, but then rises up to $T = 0.2$ in the next bin, and then falls once more below $T = 0.1$ at 6.4 Mpc. This behavior of $T > 0.1$ peaks beyond the distance where T first drops below 0.1 is also seen in the near-zones of some SDSS quasars (Fan et al. 2006b) and in the simulated quasar line of sight of Bolton & Haehnelt (2007a), and is likely due to the existence of low-density regions within the quasar near-zone. Statistically significant transmission below the $T = 0.1$ level is detected in bins at distances up to 12.7 Mpc. Given these observations, what should we conclude about the size of the highly ionized near-zone surrounding this quasar?

To further understand the properties of the near-zone we also show the binned Lyβ transmission in Figure 8 (*middle*). These data have been statistically corrected for foreground Lyα absorption. Excluding the first few megaparsecs, there is statistically significant Lyβ transmission all the way out to 12.7 Mpc. In fact, the Lyβ optical depth in this region is considerably lower than expected given the observed Lyα optical depth, which suggests the foreground Lyα forest at $z \approx 4.9$ along this line of sight is unusually transparent.

Figure 8 (*top*) shows the Lyα and Lyβ transmission (this time without statistical correction of the foreground Lyα forest) of the full-resolution spectrum without binning. There is a correspondence between positive features in Lyα and Lyβ at most places, although the correspondence in width and height of these features varies due to the varying foreground Lyα absorption. The transmission feature at 12 Mpc is clearly visible in Lyβ. From the weakness of this feature at Lyα we conclude that the Lyβ feature is due to both a low-density region near the quasar and an unusually transparent patch at $z \approx 4.9$. We note, as emphasized by Songaila (2004), that if flux is detected at all at Lyα, it is better to adopt this measurement than to trust the apparently higher S/N Lyβ measurement because of uncertainty in the foreground subtraction. Nevertheless, the detection of positive flux in all Lyα bins out to 12.7 Mpc suggests that this is the true size of the zone impacted by the quasar ionizing flux. This is significantly greater than the 6.4 Mpc that would result from imposing a $T < 0.1$ criterion.

Throughout the above discussion we have assumed that the flux detected is not due to transparency caused by a very low neutral fraction ($f_{\rm H\,I} < 10^{-4}$) in the IGM beyond the quasar ionization front. There are a couple of facts supporting this assumption. First, there is significant flux detected in every Lyβ bin from 3 to 12.7 Mpc and positive (although not always significant) Lyα flux in every bin. Then at larger distances, the IGM appears very opaque in Lyα and Lyβ until there is some Lyβ transmission at $\sim$20 Mpc. The transmitted flux in the region 6.4–12.7 Mpc corresponds to an effective Lyα optical depth of $\tau = 3.0$. This is to be compared with the optical depth at a similar redshift (this region is $5.92 < z < 6.02$) and bin size along the lines of sight to all four highest redshift SDSS quasars of $\tau > 4.3$ (Fan et al. 2006b). If the transmission at 6.4–12.7 Mpc is beyond the quasar ionization front, then the IGM here has an unusually high ionizing background over a substantial redshift range.

Figure 8 (*bottom*) shows the Lyα transmission close to CFHQS J2329−0301. The spectrum does not have a high enough S/N to provide useful Lyβ data. The Lyα near-zone is remarkably similar to that of CFHQS J1509−1749, with the transmission first

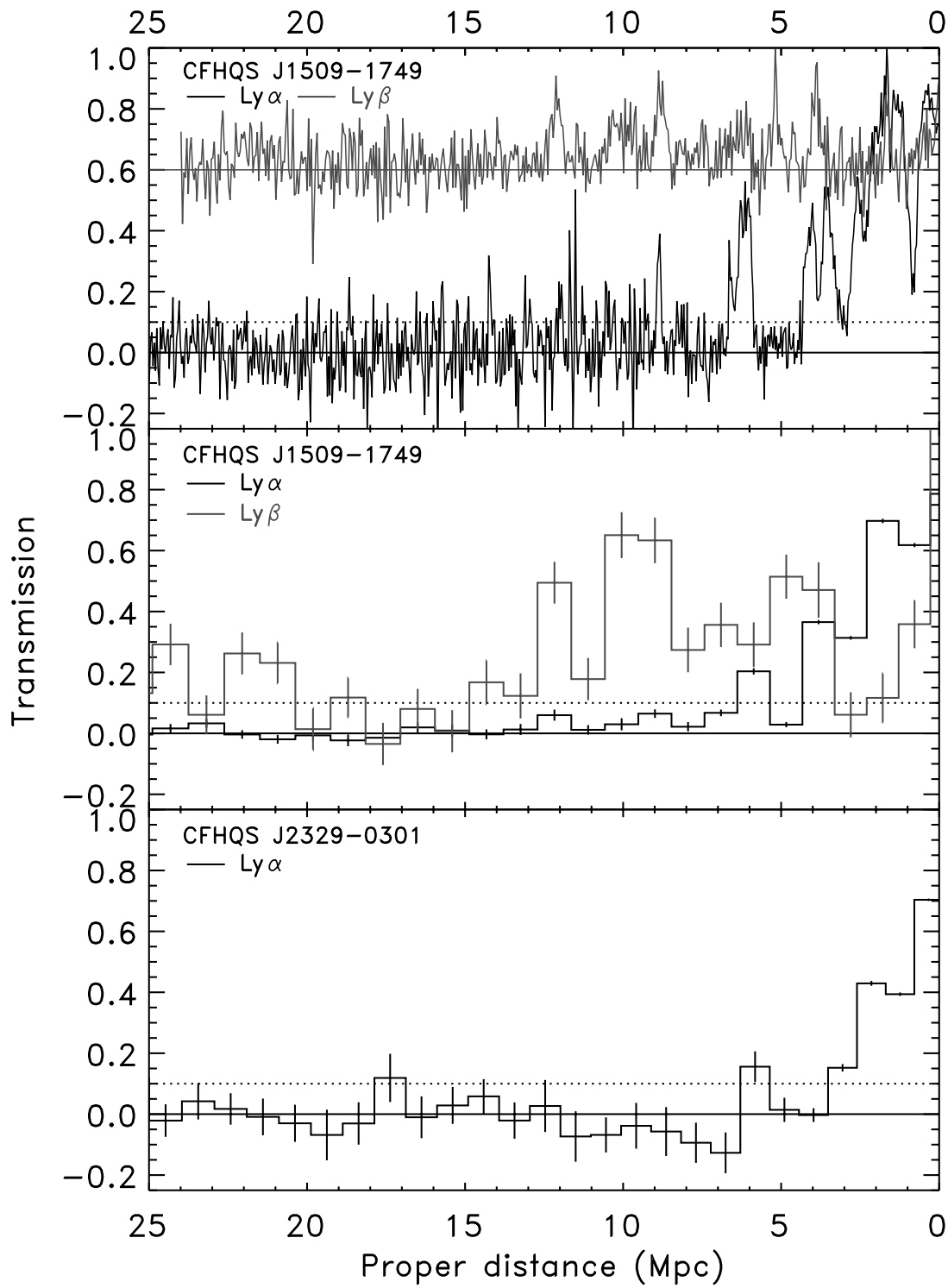

FIG. 8.—Lyman transmission close to the quasar redshift for CFHQS J1509−1749 (*top two panels*) and CFHQS J2329−0301 (*bottom*). The horizontal scale shows the distance in physical coordinates from the quasar. The top panel shows the Lyα and Lyβ unbinned spectra for CFHQS J1509−1749. The Lyβ transmission has not been corrected for foreground Lyα absorption and is shown vertically offset by +0.6 for clarity. The middle panel shows the same data but binned in 20 Å bins, with Lyβ now corrected for foreground Lyα absorption. The bottom panel shows 20 Å binned Lyα transmission for CFHQS J2329−0301. The dotted horizontal lines show $T = 0.1$. [*See the electronic edition of the Journal for a color version of this figure.*]

dropping below $T = 0.1$ at a distance of 3.7 Mpc, followed by a spike with $T > 0.1$, and then falling below $T = 0.1$ again at 6.3 Mpc. Due to the lower S/N of the data we would not be able to detect any peaks at larger distances of comparable strength to those in CFHQS J1509−1749.

The CFHQS quasars are mostly of lower luminosity than those of the SDSS, so we must scale our near-zone sizes to a common luminosity before comparison with SDSS quasars and simulations carried out to match SDSS quasars. We scale the sizes to the equivalent for $M_{1450} = -27$, assuming $R \propto \dot{N}^{1/3}$. Because CFHQS J1509−1749 has $M_{1450} = -26.98$, no luminosity scaling is necessary. For CFHQS J2329−0301, with $M_{1450} = -25.23$, the near-zone size of 6.3 Mpc goes up to 10.8 Mpc after luminosity scaling.

We can compare the luminosity-scaled sizes of the CFHQS near-zones with those from the more luminous SDSS quasars. Bolton & Haehnelt (2007b) give the luminosity-scaled sizes of the Lyα near-zones measured from the four SDSS quasars at $z > 6.1$ (excluding the broad absorption line quasar SDSS J1048+4607) using a definition similar to ours: the last pixel where $T > 0.1$. The four SDSS near-zone sizes are 2.6, 4.8, 6.2, and 13.6 Mpc. Our two CFHQS sizes of 6.4 and 10.8 Mpc are within the range of the SDSS quasars, somewhat toward the upper end of the distribution.

Although there are many uncertainties associated with using the near-zone sizes to estimate the neutral fraction of the IGM that the quasar ionization front expands into, the finding of relatively large near-zone sizes in the two CFHQS quasars does allow us to determine some constraints. First, as shown by Bolton & Haehnelt (2007a) there is little dependence on the quasar lifetime if $f_{\rm H\,I} \lesssim 0.1$ and/or at $t_Q \gtrsim 10^7$ yr, because in these cases the observed near-zone size depends not on the expanding ionization front but on the residual neutral hydrogen left behind the ionization front. Both short lifetimes and high neutral fractions lead to small near-zone sizes, so we can safely assume that quasar lifetime is not a factor. Bolton & Haehnelt (2007b) simulated many quasar lines of sight with parameters of $M_{1450} = -27$ and $t_Q = 10^7$ yr. They found that for $f_{\rm H\,I} > 0.3$ the near-zone sizes are all <4.5 Mpc. At $f_{\rm H\,I} = 0.1$ the average near-zone size is 4.5 Mpc, with a range up to 6.5 Mpc. The only simulated near-zone sizes greater than 10 Mpc come from simulations with $f_{\rm H\,I} < 10^{-3}$.

The luminosity-scaled sizes for the two CFHQS quasar near-zones are 6.4 and 10.8 Mpc. Therefore, we can be quite confident that neither quasar is located in an IGM with $f_{\rm H\,I} > 0.3$. For CFHQS J2329−0301 at $z = 6.43$ with a luminosity-scaled near-zone size of 10.8 Mpc, a very highly ionized IGM is inferred. Even if the quasar redshift has been overestimated by $\delta z = 0.02$, then the observed near-zone size of 5.2 Mpc would still give a luminosity-scaled size of 9.0 Mpc. For both quasars the quasar radiation is emitted into a substantially preionized IGM. This indicates that these locations had already been reionized to $f_{\rm H\,I} < 0.3$ at their respective redshifts of $z = 6.12$ and 6.43. Several authors have suggested that because luminous quasars are expected to form in rare overdense regions, the surrounding IGM had already been preionized by galaxies (Yu & Lu 2005; Alvarez & Abel 2007; Lidz et al. 2007). The possibility that quasar near-zones do not represent typical regions of the IGM must always be kept in mind when interpreting results such as these. However, we note that the lower luminosities of most CFHQS quasars, such as CFHQS J2329−0301, mean that they are expected to be powered by less massive black holes hosted in less rare, lower mass dark matter halos, reducing the likelihood of preionization by cluster galaxies.

6. CONCLUSIONS

We have presented the discovery of four new CFHQS quasars at $z > 6$. These were discovered from incomplete follow-up of less than half the final survey area, and we expect many more quasars to be found in the next few years. We have discussed the observed properties of the quasars, including emission lines, intervening absorption lines, continuum slopes, and dust reddening.

Sensitive millimeter continuum observations have been carried out with MAMBO at the IRAM 30 m telescope. One of the four quasars has been securely detected. Its strong dust continuum is likely due to a high star formation rate in its host galaxy. The mean 1.2 mm flux of the CFHQS quasars is substantially lower than the mean 1.2 mm flux of SDSS quasars at similar redshifts. This is indicative of a luminosity dependence of the dust continuum emission.

We have investigated the constraints that the discovery spectra can put on the ionization state of the IGM. For all but one quasar, higher S/N spectroscopy is required to perform a full analysis of the IGM properties.

CFHQS J1509−1749 at $z = 6.12$ shows significant IGM optical depth evolution from $z = 5$ to 6. The highest redshift bin at $5.75 < z < 5.90$ has an effective optical depth of $\tau_{\rm Ly\alpha} \approx 5$, which is one of the highest effective optical depths found at this redshift and consistent with a factor of 3 increase in $f_{\rm H\,I}$ from $z = 5$.

Both CFHQS J1509−1749 and CFHQS J2329−0301 have large, highly ionized near-zones of at least 6 proper Mpc. These large near-zones are inconsistent with quasar ionization fronts expanding into a highly neutral ($f_{\rm H\,I} \gtrsim 0.3$) IGM (Bolton & Haehnelt 2007b). Our results are broadly consistent with the (mass-averaged) value of $f_{\rm H\,I} \sim 0.04$ at $z \sim 6.4$ determined by Fan et al. (2006b) from the evolution of SDSS quasar near-zone sizes. Our strongest constraint is from CFHQS J2329−0301 at $z = 6.43$, which has a luminosity-scaled near-zone size of 10.8 Mpc, which is only consistent with $f_{\rm H\,I} < 10^{-3}$. In addition, the lower luminosity of this quasar compared to SDSS quasars makes it less likely that its surroundings were preionized by cluster galaxies.

Taken together, the results of (1) a significant increase in the IGM optical depth at $z \approx 5.8$ (for CFHQS J1509−1749 and also observed in the SDSS) and (2) the low neutral fractions inferred from the near-zones of CFHQS (and some SDSS) $z > 6.1$ quasars suggest that reionization is well under way before $z = 6.4$ but is still not complete by $z = 5.7$. This is a more extended period than obtained from most simple models where overlap occurs rapidly.

Finally, we note that cosmic variance is still a significant issue for the highest redshift quasars and that many more quasars at $z > 6.1$ are required to accurately determine the IGM evolution at $z > 6$.

This work is based on observations obtained with MegaPrime/MegaCam, a joint project of the Canada-France-Hawaii Telescope (CFHT) and CEA/DAPNIA, at the CFHT, which is operated by the National Research Council (NRC) of Canada, the Institut National des Sciences de l'Univers of the Centre National de la Recherche Scientifique (CNRS) of France, and the University of Hawaii. This work is based in part on data products produced at TERAPIX and the Canadian Astronomy Data Centre as part of the Canada-France-Hawaii Telescope Legacy Survey (CFHTLS), a collaborative project of NRC and CNRS. This work is also based on observations obtained at the Gemini Observatory, which is operated by the Association of Universities for Research in Astronomy, Inc., under cooperative agreement with the NSF on behalf of the Gemini partnership: the National Science Foundation (United States), the Particle Physics and Astronomy Research Council (United Kingdom), the National Research Council (Canada), CONICYT (Chile), the Australian Research Council (Australia), CNPq (Brazil), and CONICET (Argentina). This paper uses data from Gemini programs GS-2006A-Q-16, GS-2006A-Q-38 and GS-2006B-Q-17. The Hobby-Eberly Telescope (HET) is a joint project of the University of Texas at Austin, Pennsylvania State University, Stanford University, Ludwig-Maximillians-Universitaet Muenchen, and Georg-August-Universitaet Goettingen. The HET is named in honor of its

principal benefactors, William P. Hobby and Robert E. Eberly. The Marcario Low Resolution Spectrograph was developed by the HET partnership and the Instituto de Astronomia, Universidad Nacional Autonoma de Mexico. The Marcario LRS is named for Mike Marcario of High Lonesome Optics, who fabricated several optics for the instrument but died before its completion. This work is also based on observations made with the ESO New Technology Telescope at the La Silla Observatory, and on observations at the Kitt Peak National Observatory, National Optical Astronomy Observatory, which is operated by the Association of Universities for Research in Astronomy, Inc., under cooperative agreement with the NSF. This work is also based on observations made with the Nordic Optical Telescope, operated on the island of La Palma jointly by Denmark, Finland, Iceland, Norway, and Sweden in the Spanish Observatorio del Roque de los Muchachos of the Instituto de Astrofisica de Canarias, and on observations with the IRAM 30 m Millimeter Radio Telescope at Pico Veleta. IRAM is supported by INSU/CNRS (France), MPG (Germany), and IGN (Spain). This research has made use of the NASA/IPAC Extragalactic Database, which is operated by the Jet Propulsion Laboratory, California Institute of Technology, under contract with the National Aeronautics and Space Administration. Support for M. G. was under REU program grant NSF AST 02-43745. We thank the queue observers at CFHT, Gemini, HET, and IRAM who obtained data for this paper, and Matthew Shetrone for coordinating the HET observations. We also thank J. J. Kavelaars for advice on planning our MegaCam observations in the CFHTLS Very Wide survey region, and Nick Gnedin for providing the results of his simulations in electronic form. We finally thank the anonymous referee for suggestions which improved this paper.

APPENDIX

FINDING CHARTS

Figure 9 presents $3' \times 3'$ finding charts for the CFHQS quasars. All images are centered on the quasars and have the same orientation on the sky. These are the MegaCam z'-band images in which the quasars were first identified. MegaCam has gaps between the CCDs, and these data were not dithered, so the gaps remain and are evident in the top two images where the quasars lie close to the edge of a CCD. For all quasars except CFHQS J1509−1749, the MegaCam data are from a single exposure, leading to many cosmic rays in the final images.

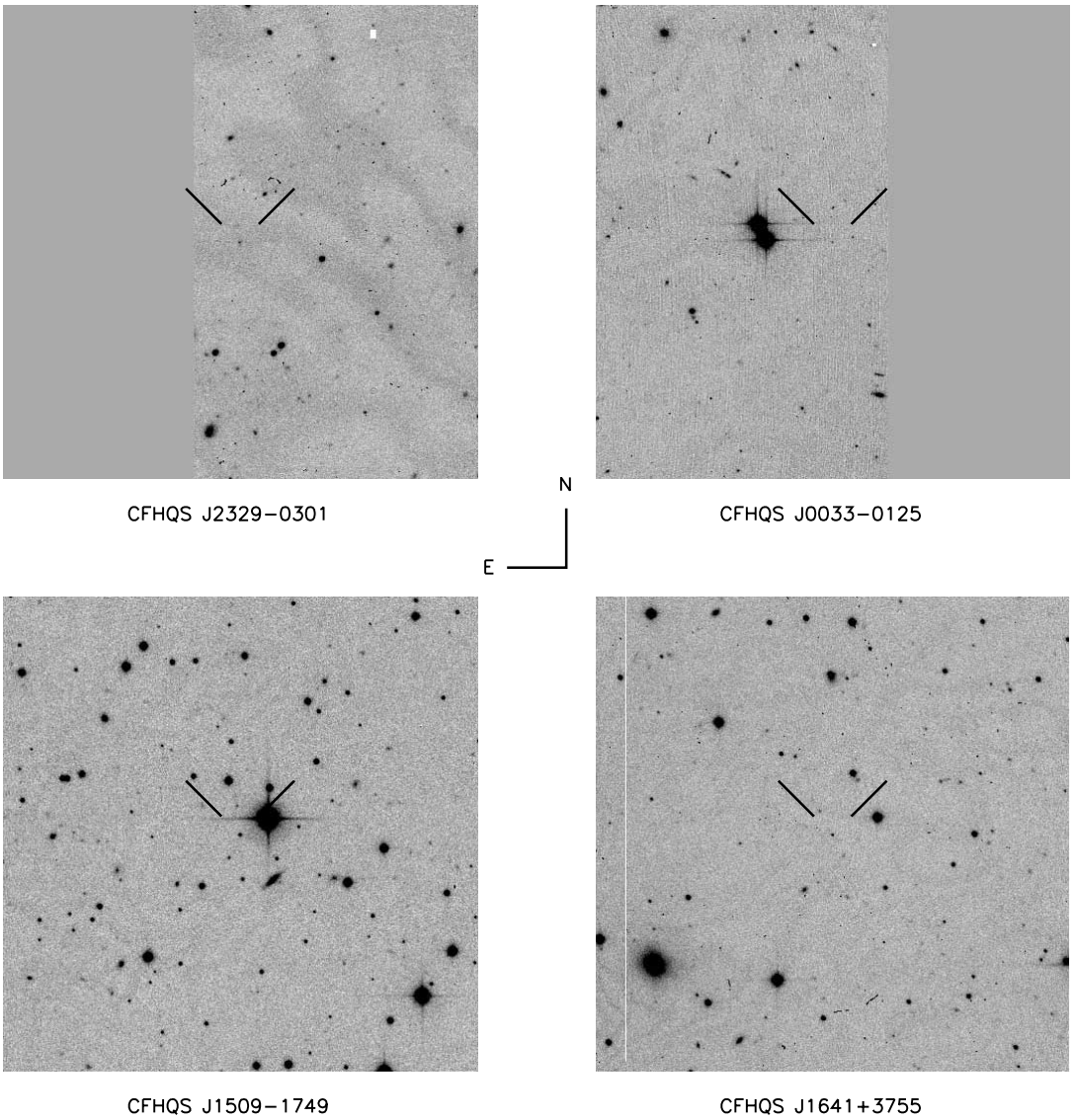

FIG. 9.—The z'-band finding charts for the CFHQS quasars.

REFERENCES

Abraham, R. G., et al. 2004, AJ, 127, 2455
Adelberger, K. L., & Steidel, C. C. 2005, ApJ, 627, L1
Alexander, D. M., Smail, I., Bauer, F. E., Chapman, S. C., Blain, A. W., Brandt, W. N., & Ivison, R. J. 2005, Nature, 434, 738
Alvarez, M. A., & Abel, T. 2007, MNRAS, 380, L30
Barkana, R., & Loeb, A. 2001, Phys. Rep., 349, 125
Becker, G. D., Rauch, M., & Sargent, W. L. 2007, ApJ, 662, 72
Becker, G. D., Sargent, W. L., Rauch, M., & Simcoe, R. A. 2006, ApJ, 640, 69
Becker, R. H., White, R. L., & Helfand, D. J. 1995, ApJ, 450, 559
Becker, R. H., et al. 2001, AJ, 122, 2850
Beelen, A. 2004, Ph.D. thesis, Obs. Paris
Beelen, A., Cox, P., Benford, D. J., Dowell, C. D., Kovacs, A., Bertoldi, F., Omont, A., & Carilli, C. L. 2006, ApJ, 642, 694
Bertin, E., & Arnouts, S. 1996, A&AS, 117, 393
Bertoldi, F., et al. 2003a, A&A, 406, L55
———. 2003b, A&A, 409, L47
Bolton, J. S., & Haehnelt, M. G. 2007a, MNRAS, 374, 493
———. 2007b, MNRAS, 381, L35
Bromley, J. M., Somerville, R. S., & Fabian, A. C. 2004, MNRAS, 350, 456
Cen, R., & Haiman, Z. 2000, ApJ, 542, L75
Comerford, J. M., Haiman, Z., & Schaye, J. 2002, ApJ, 580, 63
Cox, P., et al. 2005, in The Dusty and Molecular Universe: A Prelude to Herschel and ALMA, ed. A. Wilson (Noordwijk: ESA), 115
Djorgovski, S. G., Castro, S., Stern, D., & Mahabal, A. A. 2001, ApJ, 560, L5
Elias, J. H., Rodgers, B., Joyce, R. R., Lazo, M., Doppmann, G., Winge, C., & Rodriguez-Ardila, A. 2006, Proc. SPIE, 6269, 36
Fan, X., et al. 2000, AJ, 120, 1167
———. 2001, AJ, 122, 2833
———. 2003, AJ, 125, 1649
———. 2006a, AJ, 131, 1203
———. 2006b, AJ, 132, 117
Gehrz, R. D. 1989, in IAU Symp. 135, Interstellar Dust, ed. L. J. Allamandola & A. G. G. M. Tielens (Dordrecht: Kluwer), 445
Gnedin, N. Y., & Fan, X. 2006, ApJ, 648, 1
Hall, P. B., et al. 2002, ApJS, 141, 267
Hill, G. J., Nicklas, H. E., MacQueen, P. J., Tejada, C., Cobos Duenas, F. J., & Mitsch, W. 1998, Proc. SPIE, 3355, 375
Hook, I., Jorgensen, I., Allington-Smith, J. R., Davies, R. L., Metcalfe, N., Murowinski, R. G., & Crampton, D. 2004, PASP, 116, 425
Hopkins, P. F., et al. 2004, AJ, 128, 1112
King, A. R., & Pringle, J. E. 2006, MNRAS, 373, L90
Kreysa, E., et al. 1998, Proc. SPIE, 3357, 319
Lidz, A., McQuinn, M., Zaldarriaga, M., Hernquist, L., & Dutta, S. 2007, ApJ, submitted (astro-ph/0703667)
Magorrian, J., et al. 1998, AJ, 115, 2285
Maiolino, R., Schneider, R., Oliva, E., Bianchi, S., Ferrara, A., Mannucci, F., Pedani, M., & Roca Sogorb, M. 2004, Nature, 431, 533
Maiolino, R., et al. 2005, A&A, 440, L51
McGreer, I. D., Becker, R. H., Helfand, D. J., & White, R. L. 2006, ApJ, 652, 157
McLure, R. J., Jarvis, M. J., Targett, T. A., Dunlop, J. S., & Best, P. N. 2006, MNRAS, 368, 1395
Mesinger, A., & Haiman, Z. 2007, ApJ, 660, 923
Miralda-Escudé, J., Haehnelt, M., & Rees, M. 2000, ApJ, 530, 1
Nestor, D. B., Turnshek, D. A., & Rao, S. M. 2005, ApJ, 628, 637
Oh, S. P., & Furlanetto, S. R. 2005, ApJ, 620, L9
Omont, A., et al. 2001, A&A, 374, 371
———. 2003, A&A, 398, 857
Paschos, P., & Norman, M. L. 2005, ApJ, 631, 59
Peng, C. Y., Impey, C. D., Rix, H.-W., Kochanek, C. S., Keeton, C. R., Falco, E. E., Lehar, J., & McLeod, B. A. 2006, ApJ, 649, 616
Priddey, R. S., Isaak, K. G., McMahon, R. G., & Omont, A. 2003, MNRAS, 339, 1183
Prochter, G. E., Prochaska, J. X., & Burles, S. M. 2006, ApJ, 639, 766
Rao, S. M., & Turnshek, D. A. 2000, ApJS, 130, 1
Rao, S. M., Turnshek, D. A., & Nestor, D. B. 2006, ApJ, 636, 610
Rees, M. 1999, in After the Dark Ages: When Galaxies Were Young (The Universe at $2 < z < 5$), ed. S. S. Holt & E. P. Smith (College Park: AIP), 13
Richards, G. T., Vanden Berk, D. E., Reichard, T. A., Hall, P. B., Schneider, D. P., SubbaRao, M., Thakar, A. R., & York, D. G. 2002, AJ, 124, 1
Richards, G. T., et al. 2003, AJ, 126, 1131
———. 2004, AJ, 127, 1305
Robson, I., Priddey, R. S., Isaak, K. G., & McMahon, R. G. 2004, MNRAS, 351, L29
Ryan-Weber, E. V., Pettini, M., & Madau, P. 2006, MNRAS, 371, L78
Shapiro, S. L. 2005, ApJ, 620, 59
Shields, G. A., et al. 2003, ApJ, 583, 124
Solomon, P. M., & Vanden Bout, P. A. 2005, ARA&A, 43, 677
Songaila, A. 2004, AJ, 127, 2598
Spergel, D. N., et al. 2007, ApJS, 170, 377
Stratta, G., Maiolino, R., Fiore, F., & D'Elia, V. 2007, ApJ, 661, L9
Telfer, R. C., Zheng, W., Kriss, G. A., & Davidsen, A. F. 2002, ApJ, 565, 773
Todini, P., & Ferrara, A. 2001, MNRAS, 325, 726
Vanden Berk, D., et al. 2001, AJ, 122, 549
van Dokkum, P. G. 2001, PASP, 113, 1420
Volonteri, M., & Rees, M. J. 2005, ApJ, 633, 624
Walter, F., et al. 2003, Nature, 424, 406
———. 2004, ApJ, 615, L17
Wang, R., et al. 2007, AJ, 134, 617
White, R. L., Becker, R. H., Fan, X., & Strauss, M. A. 2003, AJ, 126, 1
Willott, C. J., Delfosse, X., Forveille, T., Delorme, P., & Gwyn, S. 2005a, ApJ, 633, 630
Willott, C. J., McLure, R. J., & Jarvis, M. J. 2003, ApJ, 587, L15
Willott, C. J., et al. 2005b, ApJ, 626, 657
Wyithe, J. S. B., & Loeb, A. 2002, Nature, 417, 923
———. 2004, Nature, 427, 815
———. 2006, ApJ, 646, 696
Wyithe, J. S. B., Loeb, A., & Carilli, C. 2005, ApJ, 628, 575
Yoo, J., & Miralda-Escudé, J. 2004, ApJ, 614, L25
Yu, Q., & Lu, Y. 2005, ApJ, 620, 31